

A major purpose of the Technical Information Center is to provide the broadest dissemination possible of information contained in DOE's Research and Development Reports to business, industry, the academic community, and federal, state and local governments.

Although a small portion of this report is not reproducible, it is being made available to expedite the availability of information on the research discussed herein.

Los Alamos National Laboratory is operated by the University of California for the United States Department of Energy under contract W-7405-ENG-36

LA-UR--86-3946

DE87 002901

TITLE: CALCULATION OF ELECTROMAGNETIC  
OBSERVABLES IN FEW-BODY SYSTEMS

AUTHOR(S): B. F. Gibson

**MASTER**

SUBMITTED TO: Invited lecture to be published in the Proceedings  
of the Autumn School on Few-Body Methods, University  
of Lisbon, Lisbon, Portugal, October 13-21, 1986

**DISCLAIMER**

This report was prepared as an account of work sponsored by an agency of the United States Government. Neither the United States Government nor any agency thereof, nor any of their employees, makes any warranty, express or implied, or assumes any legal liability or responsibility for the accuracy, completeness, or usefulness of any information, apparatus, product, or process disclosed, or represents that its use would not infringe privately owned rights. Reference herein to any specific commercial product, process, or service by trade name, trademark, manufacturer, or otherwise does not necessarily constitute or imply its endorsement, recommendation, or favoring by the United States Government or any agency thereof. The views and opinions of authors expressed herein do not necessarily state or reflect those of the United States Government or any agency thereof.

By acceptance of this article the publisher recognizes that the U.S. Government retains a nonexclusive, royalty-free license to publish or reproduce the published form of this contribution or to allow others to do so, for U.S. Government purposes.

The Los Alamos National Laboratory requests that the publisher identify this article as work performed under the auspices of the U.S. Department of Energy.

**Los Alamos** Los Alamos National Laboratory  
Los Alamos, New Mexico 87545

# CALCULATION OF ELECTROMAGNETIC OBSERVABLES IN FEW-BODY SYSTEMS

B.F. Gibson

School of Physics  
University of Melbourne  
Parkville Victoria 3052  
Australia

and

Theoretical Division\*  
Los Alamos National Laboratory  
Los Alamos, New Mexico, 87545  
U.S.A.

An introduction to the calculation of electromagnetic observables in few-body systems is given by studying two examples in the trinucleon system: 1) the elastic electron scattering charge form factor in configuration space and momentum space and 2) the two-body photodisintegration of  $^3\text{H}$  leading to a neutron-deuteron final state in a separable potential formalism. In the discussion of charge form factor calculations, a number of related topics are touched upon: the relation of structure in  $\Psi$  to the properties of simple NN forces, the Faddeev and Schrödinger solution to the harmonic oscillator problem, the Rosenbluth formula for electron scattering from a spin-1/2 nuclear target (e.g., the proton or  $^3\text{He}$ ), and the charge density operator. Formulae for  $^3\text{He}$  and  $^3\text{H}$  charge form factors in a central force approximation are given in configuration and momentum space. The physics of these form factors is discussed in light of results from realistic nucleon-nucleon potential model calculations, including the effects of two-pion-exchange three-body force models. Topics covered are the rms charge radii, characterization of the charge form factors, properties of the charge densities, and the Coulomb energy of  $^3\text{He}$ . In the discussion of the  $^3\text{H}$  photodisintegration, the Siegert form of the electric dipole operator (in the long wave length limit) is derived as are the separable potential equations which describe the off-shell transition amplitudes which connect nucleon-plus-corrected-pair states. Expressions for the Born amplitudes required to complete the two-body photodisintegration amplitude calculation are given. Numerical results for a model central force problem are discussed and compared with an approximate calculation. Comparisons with  $^3\text{H}(\gamma, n)d$  and  $^3\text{He}(\gamma, p)d$  data are made, and the significant features of the exact theoretical calculation are outlined.

\*Permanent address

## LECTURE I. TRINUCLEON FORM FACTORS FROM ELASTIC ELECTRON SCATTERING

### I. Introduction

Now that we have learned how to generate few-body wave functions in numerous ways, let us explore how one relates these ideas to the physical world of experimental observables. Most of us approach the everyday world around us by means of five senses. Of these, one of the most important is sight. How do we see? Photons from a source (natural or artificial) are scattered from objects and detected by our eyes. Experience has taught our super computer brains how to process the electronic signals generated by the optic nerve into meaningful images. Photon scattering is one of our oldest analytical tools.

Photon scattering is not the only such process that provides us with meaningful information about the world around us. Each of you is familiar with the story of Rutherford scattering and the discovery of the nucleus. In that case, alpha particle scattering revealed that the atom was not a uniform charge distribution. That example contains an important lesson: new physics is discovered when experimental observation differs from the result of a model calculation that is as complete as possible in terms of the known, relevant physics - not when undetermined parameters are varied (or chosen) to put a curve through the data. The purpose of calculations performed within the context of an exact theory is to explain honest differences with otherwise successful approximate theoretical prescriptions and to elucidate or discover novel aspects of physics.

The simplest picture of the nucleus is obtained in much the same manner as we use light to see, although we employ the "virtual photon" exchanged between an electron and the nucleus in the electron scattering process to define our image. Using elastic electron scattering, one can explore the charge and magnetic moment densities of the nucleus. The relativistic theory was first written down in the early 1930's by Mott.<sup>1</sup> The fact that nuclear charge distributions and sizes could be extracted from such experiments was laid out clearly by Rose<sup>2</sup> in the late 1940's. It was in the 1950's that elastic electron scattering became a feasible experimental tool<sup>3</sup> and Hofstadter won the Nobel Prize in 1961 for his work in electron scattering investigations of the structure of the nucleus. It is from this background that we ask such questions as whether we can provide a quantitative model of the charge and magnetic moment distributions of the few-nucleon systems - those nuclei whose wave functions we can generate from nonrelativistic Hamiltonians incorporating realistic representations of the nucleon-nucleon interaction.

## II. Qualitative Aspects of the Relation between $\Psi$ and $V$

Because one is investigating a density or  $|\Psi|^2$  function in studying the differential cross section measured in unpolarized elastic electron scattering, the historical approach to analysis of the data has been to postulate a plausible analytic form for the density and to ask how well the data can be described by varying the model parameters. Such a procedure should be utilized with caution, because it is clear from the Schrödinger equation

$$[T + V] \Psi = E \Psi \quad (1)$$

that important features of the nucleon-nucleon interaction will be reflected in the wave function  $\Psi$  and therefore in the density  $|\Psi|^2$ . Assuming a given form for  $\Psi$  makes a definite statement about the underlying Hamiltonian which has been implicitly assumed.

Let us examine the spatially symmetric S-state components that result from using three different central potential forms to generate the trinucleon wave function: smooth Gaussian (G), one term Yukawa (MT IV model of Malfliet and Tjon<sup>4</sup>), and a two term Yukawa with short-range repulsion (MT V model of Malfliet and Tjon<sup>4</sup>). Figure 1 depicts the Schrödinger wave function for the G model where  $\vec{x}$  and  $\vec{y}$  are the Jacobi coordinates of the  $^3\text{H}$  system and  $\theta$  is the angle between the two vectors.<sup>5</sup> (See Appendix A.) As expected,  $\Psi$  for this smooth potential shows no sharp structure. This wave function is reminiscent of that which results from solving the harmonic oscillator (HO) Hamiltonian. However, it differs in that the wave function falls off exponentially. (We shall return to the HO problem below.) The point to retain is that a smooth ad hoc wave function assumption implies an assumption that the underlying two-body potential is reasonably smooth. This point is emphasized by comparing Fig.1 with Fig.2, in which we plot  $\Psi$  for the MT IV potential model.<sup>5</sup> The  $\Psi$  for the Yukawa potential exhibits a definite kink, or ridge structure, due to the  $1/x$  singularity of the Yukawa form. When  $y = x/2$ , one pair of interacting nucleons lie close together and the  $1/x$  singularity leads to a discontinuity in the first derivative of  $\Psi$  along that line. This occurs for  $\theta=0$ , a collinear configuration, but not for  $\theta=90^\circ$ , an isosceles triangle configuration, in which overlapping pairs cannot occur for  $x \neq 0 \neq y$ . The ridge structure is even more apparent in the small S'-state components of  $\Psi$ , when the singlet and triplet potentials differ, as shown in Fig.3, where one of the S'-state components is plotted for the MT II-IV model. Thus, even a purely attractive

potential having a simple Yukawa singularity leads to structure in the Schrödinger wave function.

Let us turn to the MT V model with short-range repulsion, whose wave function is plotted<sup>5</sup> in Fig.4. One anticipates that  $\Psi$  will be small whenever any two of the nucleons are close together. Clearly this has led to the "death valley" in  $\Psi$  along  $y = x/2$  and along  $x=0$ .

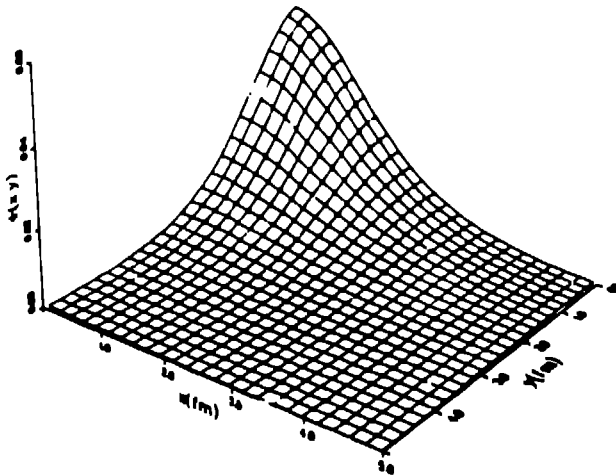


Fig.1 The Schrödinger wave function at fixed angle  $\theta=0^\circ$  for the Gaussian potential model.

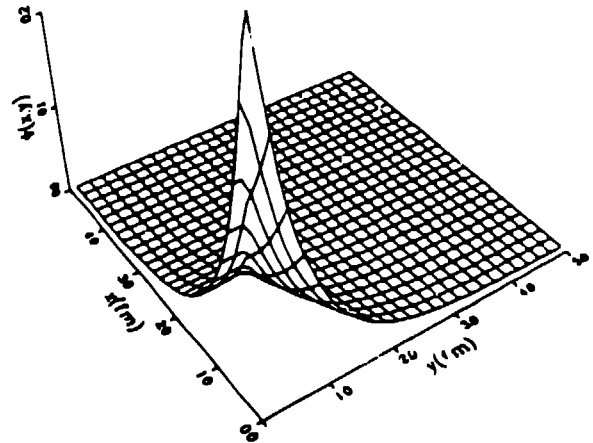


Fig.2 The Schrödinger wave function at fixed angle  $\theta=0^\circ$  for the Yukawa potential (MT IV).

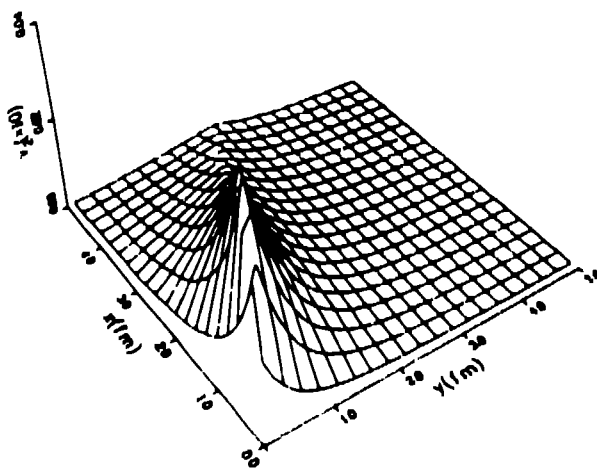


Fig.3 The Schrödinger wave function component  $1/Z$  of the  $\psi'$ -state at fixed angle  $\theta=0^\circ$  for the MT II-IV potential model.

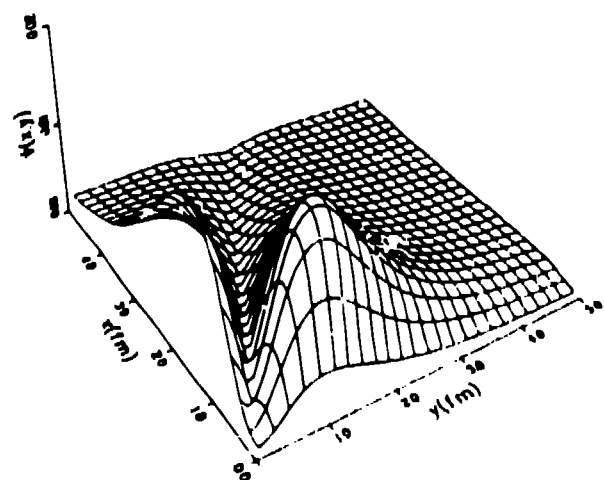


Fig.4 The Schrödinger wave function at fixed angle  $\theta=0^\circ$  for the MT V potential model.

The two peaks in  $\Psi$  correspond to configurations in which the three nucleons are separated by about 1 fm, the distance at which the MT V potential attains its greatest depth (maximum attraction). For  $\theta=0^\circ$  (not shown) these two peaks merge into one corresponding to an equilateral triangle configuration with internucleon separations of about 1 fm. Note that  $\Psi$  for the MT V model is suppressed near the origin, in contrast to  $\Psi$  for purely attractive potentials which has a maximum at the origin. In the neighborhood of  $x=y=0$ , all three particles are close together and the short-range repulsion of the potential has its maximum effect.

We have seen that as the potential model becomes more sophisticated, the complexity of the corresponding trinucleon wave function increases. Yukawa forms introduce kinks or ridges. Short-range repulsion produces peaks and valleys as the nucleons localize at positions corresponding to maximum attraction in the potential. It is also clear that simple (smooth) ad hoc model wave function hypotheses imply hidden assumptions about the smoothness (lack of repulsion) of the underlying potentials. "Forewarned is forearmed".

These effects in  $\Psi$  are reflected in calculated observables; e.g., the electron scattering cross sections. To illustrate this point, we show in Fig.5 Born approximation model results for scattering off gold using charge distributions of the uniform [ $\rho(r) = \rho_0$ ,  $r < r_0$ ] and exponential [ $\rho(r) = \rho_0 e^{-r/a}$ ] forms.<sup>3,6</sup> As the surface of the distribution becomes sharper, nodes develop; the spacing of the zeros is determined effectively by the size of the system. Note that a Gaussian charge distribution leads to a straight line on such a plot. As we shall see later, the trinucleon data (and alpha particle data as well) do not support the choice of such a simple, smooth model wave function.

Because I have emphasized structure and because we have heard so much of calculating Faddeev amplitudes, let us return to the harmonic oscillator model to ensure that the distinction between Schrödinger wave function and Faddeev amplitude is clear. It is the structure in the former that influences calculated observables. Structure in the latter may have absolutely no effect upon the observables.

Each of you is familiar with the Schrödinger wave function solution to the nonrelativistic harmonic oscillator problem for three spinless particles: (here we redefine  $\hat{y}$  to be  $\sqrt{3}/2 \hat{y}$ )

$$[E + \frac{1}{M} (\hat{p}_x^2 + \hat{p}_y^2)] \Psi = \frac{B^2}{M} (\hat{x}^2 + \hat{y}^2) \Psi . \quad (2a)$$

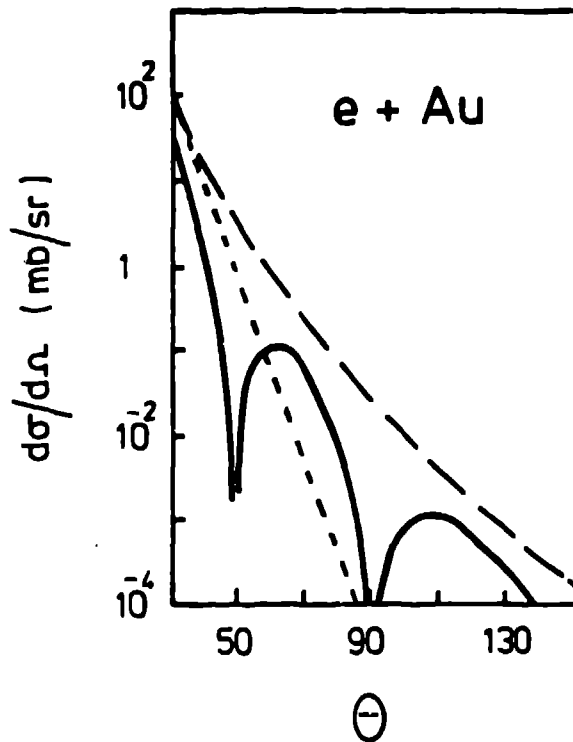


Fig.5 Cross section angular distributions for electron scattering from gold for a uniform charge distribution (solid line) an exponential charge distribution (dashed line) and a Gaussian charge distribution (dotted line).

The three-body solution is easily verified to be the familiar Gaussian function

$$\psi = 3e^{-\beta(\vec{x}^2 + \vec{y}^2)/2}, \quad (2b)$$

where  $E = 2\beta N/M$ . (See Fig.6) One can generate this solution by solving the corresponding Faddeev equation<sup>7</sup>

$$[E + \frac{1}{M}(\vec{\partial}_x^2 + \vec{\partial}_y^2)]\psi = V\psi = \frac{2\beta^2}{3M}x^2\psi \quad (3a)$$

for the Faddeev amplitude  $\psi(\vec{x}, \vec{y})$  and then constructing the Schrodinger wave function from

$$\begin{aligned} \psi(\vec{x}, \vec{y}) &= \psi(\vec{x}, \vec{y}) + \psi(\frac{1}{2}\vec{x} + \vec{y}, -\frac{3}{4}\vec{x} - \frac{1}{2}\vec{y}) \\ &\quad + \psi(-\frac{1}{2}\vec{x} - \vec{y}, -\frac{3}{4}\vec{x} - \frac{1}{2}\vec{y}) . \quad (3b) \\ &= \psi_1 + \psi_2 + \psi_3 . \end{aligned}$$

This has been done, but one can also obtain a solution for  $\psi$  if, as in this case,  $\psi$  is already known by solving the equation

$$[2\beta N + \vec{\partial}_x^2 + \vec{\partial}_y^2]\psi = 2\beta^2 x^2 e^{-\beta(\vec{x}^2 + \vec{y}^2)/2} . \quad (4a)$$

The solution is of the form

$$\psi = \Psi + \xi$$

$$= e^{-\beta \rho^2 / 2} + \frac{\beta (\hat{x}^2 - \hat{y}^2)}{2\rho^{N+1}} [\lambda J_{N+1}(\sqrt{2N\beta} \rho) + \pi Y_{N+1}(\sqrt{2N\beta} \rho) \int_0^\rho dt t^{N+2} e^{-t^2/2} J_{N+1}(\sqrt{2N\beta} t) - \pi J_{N+1}(\sqrt{2N\beta} \rho) \int_0^\rho dt t^{N+2} e^{-t^2/2} Y_{N+1}(\sqrt{2N\beta} t)], \quad (4b)$$

where  $\rho^2 = \hat{x}^2 + \hat{y}^2$  and  $\lambda$  is an arbitrary constant. Obviously one has

$$\xi_1 + \xi_2 + \xi_3 = 0 \quad (5)$$

because of the  $(\hat{x}^2 - \hat{y}^2)$  factor in  $\xi_1$ ; i.e., it does not contribute to  $\Psi$  in anyway. The  $\xi$  component of  $\psi$  results because the operator in the Faddeev equation Eq.(3a) is not  $L^2$ . Nonetheless, it illustrates

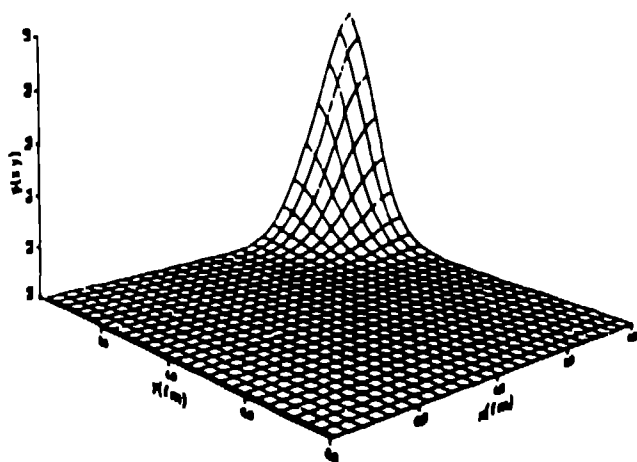


Fig.6 The Schrödinger wave function for the three-body harmonic oscillator problem.

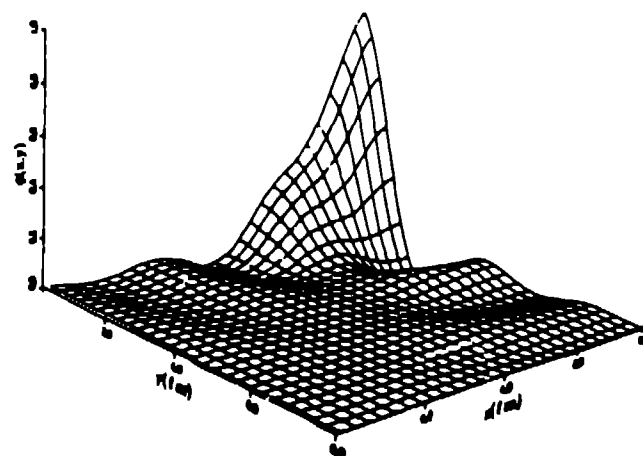


Fig.7 The Faddeev amplitude without the arbitrary component ( $\lambda=0$ ) for the three-body harmonic oscillator problem.

the point that structure in the Faddeev amplitudes (see Fig.7) may cancel in the sums needed to generate the Schrödinger wave function. (The arbitrary component of  $\psi$  has been removed by setting  $\lambda \equiv 0$ .) Compare Figures 6 and 7. In particular, the ground-state wave function for the  $A=3$  system must be positive definite, but the Faddeev amplitude for a potential with strong short-range repulsion will not be positive definite.<sup>5,8</sup> It is the cancellation between positive and

negative parts of the Faddeev amplitudes in Eq.(3b) that leads to the deep valley seen in Fig.4. Thus, one must be careful about trying to reach conclusions concerning experimental observables based on an examination of the Faddeev amplitudes for a given model. It is the full Schrödinger wave function that defines the features of the observables.

### III. Summary of Elastic Electron Scattering Formulae

Because a complete treatment of electron-proton scattering would require an hour unto itself and anything less would leave you wondering about the slight-of-hand performance, I refer you to the book by Bjorken and Drell<sup>9</sup> if the subject is not already familiar. I will quote here only the salient points and remark that they are not the subject of this lecture.

Consider the diagram shown in Fig.8 which depicts lowest order (single photon exchange) scattering of an electron from a proton. The electron with 4-momentum  $k^\mu = (\epsilon, \vec{k})$  scatters into the final state 4-momentum  $k'^\mu = (\epsilon', \vec{k}')$ , while the proton recoils from initial state with 4-momentum  $P^\mu = (E, \vec{p})$  to the final state with  $P'^\mu = (E', \vec{p}')$ . A virtual photon with 4-momentum transfer  $q^\mu = k^\mu - k'^\mu = P'^\mu - P^\mu = (\omega, \vec{q})$  is exchanged in the process. We note that  $q^2 (= q_\mu q^\mu) = \omega^2 - \vec{q}^2 < 0$ , which is space-like. Hence, electron scattering is restricted to the kinematic region for which  $\vec{q}^2 > \omega^2$ . Figure 1 describes only the exchange of a single photon, but because higher order diagrams involve higher powers of the fine structure constant  $\alpha (= 1/137)$ , the lowest order diagram should account for most of the scattering amplitude. The differential cross section for scattering an electron from a physical proton is

$$\frac{d\sigma}{d\Omega} = \sigma_M \left[ F_1^2 - \frac{\kappa_p^2 q^2}{4M^2} F_2^2 - \frac{q^2}{2M^2} (F_1 + \kappa_p F_2)^2 \tan^2 \frac{\theta}{2} \right], \quad (6)$$

where

$$\sigma_M = \left[ \frac{\alpha \cos \frac{\theta}{2}}{2\epsilon \sin^2 \frac{\theta}{2}} \right]^2 \quad (7)$$

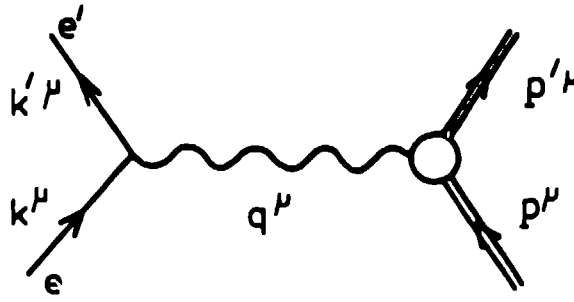


Fig.8. Lowest order diagram for electron scattering from a proton.

is the Mott cross section which describes the scattering from a point charge in the absence of any internal structure of the proton. Equation (6) is the famous Rosenbluth formula. This is the relativistic analog of the famous Rutherford cross section (with the charge of the nucleus set to 1). The  $F_1$  and  $F_2$  are structure functions associated with the charge and magnetic moment densities of the proton due to such vertex corrections as depicted in Fig.9a and 9b, and  $\kappa$  is the anomalous magnetic moment ( $\kappa_p = 1.79$  while  $\kappa_n = -1.91$ ). We note that the Dirac and Pauli structure form factors  $F_1$  and  $F_2$  can be separated experimentally by measuring the cross section as a function of  $\theta$  while holding the momentum transfer  $q$  constant.

The combinations of the form factors given by

$$G_E = F_1 + \frac{\kappa q^2}{4M^2} F_2 \quad (8a)$$

$$G_M = F_1 + \kappa F_2 \quad (8b)$$

have a more direct geometrical interpretation, and one usually finds Eq.(6) rewritten as

$$\frac{d\sigma}{d\Omega} = \frac{\sigma_M}{(1 - q^2/4M^2)} \left\{ G_E^2 - \frac{q^2}{4M^2} G_M^2 [1 + 2 \tan^2 \frac{\theta}{2} (1 - \frac{q^2}{4M^2})] \right\}. \quad (9)$$

These are the nucleon form factors that we have used in our  $^3\text{H}$  and  $^3\text{He}$  form factor studies. Numerical values were taken from the 8.2 fit of H6hler et al.<sup>10</sup>

The charge form factor  $F(q^2)$  is proportional to a matrix element of the form<sup>9</sup>

$$M \sim \int d^3p_f u(\vec{p}_f) u(\vec{p}_i) \quad (10a)$$

where  $\vec{p}_i$  and  $\vec{p}_f$  are related by  $\vec{p}_f = \vec{p}_i - \vec{q}$ . Thus, the form factor

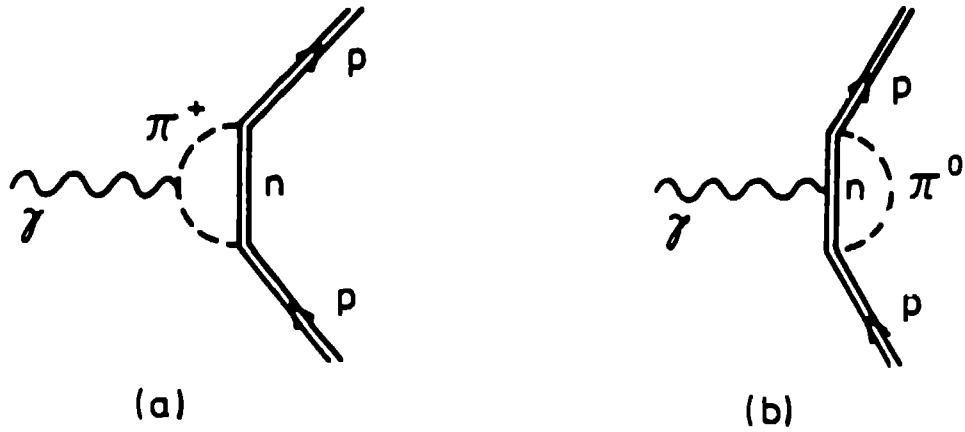


Fig. 9 Electromagnetic vertex corrections for the proton

structure function is a folding of the momentum space wave functions at the interaction vertex:

$$M \sim \int d^3p u(\vec{p} - \vec{q}) u(\vec{p}) . \quad (10b)$$

For calculations utilizing configuration space wave functions, it is more convenient to work with the Fourier transform of this expression:

$$M \sim \int d^3r e^{i\vec{q} \cdot \vec{r}} u^2(\vec{r}) . \quad (10c)$$

The  $u^2(\vec{r})$  can be identified with the charge density in the impulse approximation when one discusses nuclear systems.

The result for elastic electron scattering from the trinucleons is exactly that given by Eq.(9), because the nuclei have  $J^\pi = \frac{1}{2}^+$ . The formula for scattering from  ${}^4\text{He}$  is even simpler, because that spin-0 object has no magnetic moment. Thus one need only set  $G_M^2 \equiv 0$ . The deuteron, being a spin-1 object, is more complex; there exists an electric quadrupole density in addition to a monopole charge density, as was pointed out by Schiff<sup>11</sup> and others.<sup>3</sup> Because of the increased complexity of the formulae for the spin-1 system, they will be left as a literature search exercise for those interested.

Restricting our attention to the trinucleons, we would like to determine four form factors: a charge and a magnetic moment form factor for each of  ${}^3\text{H}$  and  ${}^3\text{He}$ . To orient ourselves, let us consider the case in which we assume that the nucleon-nucleon force is purely central. (With no tensor force, there are no D-state components in the  $A=3$  wave function.) We will also neglect differences between  ${}^3\text{He}$  and  ${}^3\text{H}$  due to the Coulomb force acting between the two protons in  ${}^3\text{He}$ . In this model, the trinucleon wave function has two components

(see Appendix B for a discussion of the spin, isospin, and spatial structure of these states.): the spatially symmetric S-state and the mixed-symmetry S'-state.<sup>12</sup> If one has solved the Faddeev amplitude equations in terms of spin-singlet and spin-triplet amplitudes  $\psi^{(s)}$  and  $\psi^{(t)}$ , then the S and S' Faddeev amplitudes are given by<sup>4,5</sup>

$$\psi^S = [\psi^{(s)} - \psi^{(t)}] / \sqrt{2} , \quad (11a)$$

$$\psi^{S'} = [\psi^{(s)} + \psi^{(t)}] / \sqrt{2} . \quad (11b)$$

Because  $\psi^{(s)}$  and  $\psi^{(t)}$  have opposite signs,  $\psi^S$  is the dominant amplitude. [If the nucleon interaction were spin independent ( $V(s) \equiv V(t)$ ), then  $\psi^{S'} \equiv 0$ .] The symmetrized combination of S-state amplitudes which define the S-state component of the Schrödinger wave function is then

$$u = \psi_1^S + \psi_2^S + \psi_3^S . \quad (12a)$$

The S'-state amplitude combinations are

$$v_1 = \frac{1}{\sqrt{6}} [\psi_2^{S'} + \psi_3^{S'} - 2 \psi_1^{S'}] , \quad (12b)$$

$$v_2 = \frac{1}{\sqrt{2}} [\psi_3^{S'} - \psi_2^{S'}] . \quad (12c)$$

The Schrödinger wave function for  ${}^3\text{He}$   $\psi = u\phi_a + (v_2\phi_1 - v_1\phi_2)$  can then be used to evaluate matrix elements of the charge density operator, which we give here in impulse approximation:

$$\begin{aligned} \rho_c = \sum_{i=1}^3 \left[ \frac{1}{2} (1 + \tau_{iz}) \rho_c^p(\vec{r} - \vec{r}_i) \right. \\ \left. + \frac{1}{2} (1 - \tau_{iz}) \rho_c^n(\vec{r} - \vec{r}_i) \right] . \end{aligned} \quad (13)$$

The  $\tau_{iz}$  are the unit isospin operators that act on the  $n$ 's in the  $\phi$ 's, as defined in Appendix B. We limit our consideration to the nonrelativistic, impulse approximation form of the charge density operator for reasons outlined in Appendix C. It suffices to note here that exchange current contributions to the charge operator are essentially relativistic corrections and they are ambiguous.<sup>13</sup> Such is not the case for the isovector exchange current contributions to the magnetic moment density, but time limitation prevents us from considering that problem here.

Because  ${}^3\text{He}$  has a charge of 2, we write its form factor as

$$2 F_c(^3\text{He}) = \langle \Psi | e^{i\vec{q} \cdot \vec{r}} \rho_c | \Psi \rangle \quad (14)$$

and evaluate Eq.(13) using the wave function  $\Psi$  defined in terms of the  $u$  and  $v$  functions of Eqs. (11 and 12). By changing variables from  $\vec{r}$  to  $\vec{r}-\vec{r}_i$ , one can factor the nucleon form factors  $G^p$  and  $G^n$  from the expression. The expectation values of the  $\tau_{iz}$  operators are easily evaluated leading to the simple relation<sup>12,14</sup>

$$2F_c(^3\text{He}) = (2G^p + G^n) F_1 - 2(G^p - G^n) F_2, \quad (15)$$

where we have defined the body form factors  $F_1$  and  $F_2$  to be

$$F_1 = \iint d^3x d^3y e^{i\frac{2}{3}\vec{q} \cdot \vec{y}} [u^2(\vec{x}, \vec{y}) + v_1^2(\vec{x}, \vec{y}) + v_2^2(\vec{x}, \vec{y})] \quad (16a)$$

and

$$F_2 = -\iint d^3x d^3y e^{i\frac{2}{3}\vec{q} \cdot \vec{y}} u(x, y) v_1(\vec{x}, \vec{y}). \quad (16b)$$

Using the corresponding wave function for  $^3\text{H}$ , we obtain in that case

$$F_c(^3\text{H}) = (G^p + 2G^n) F_1 + 2(G^p - G^n) F_2. \quad (17)$$

We have made several simplifying assumptions to obtain these expressions. Because the  $S'$  state is only a few % of the normalization, let us drop the  $v_1^2 + v_2^2$  terms in  $F_1$ . (Note that at  $\vec{q}=0$ ,  $F_2$  vanishes because  $u$  is symmetric in  $x$  and  $v_1$  is antisymmetric in  $\vec{x}$ ; thus the expressions in Eqs (14 and 16) have the proper normalizations.) Similarly, the neutron charge form factor is small, and we shall neglect it. Then we find

$$F_c(^3\text{He}) = G^p(F_1 - F_2) \quad (18a)$$

and

$$F_c(^3\text{H}) = G^p(F_1 + 2 F_2). \quad (18b)$$

Because  $F_2$  is defined in such a way as to be positive, we have  $F_c(^3\text{He}) < F_c(^3\text{H})$  for small  $q^2$  which implies that the radius of  $^3\text{He}$  must be greater than that for  $^3\text{H}$ .<sup>14</sup> We shall discuss the physics of this later, but for the moment we emphasize that it has nothing to do with Coulomb repulsion in  $^3\text{He}$ . There are no Coulomb effects in the

present analysis.

The expressions for  $F_1$  and  $F_2$  that correspond to Eq.(18) are explicitly

$$F_1(q^2) = \iiint d^3x d^3y e^{i\frac{2}{3}\vec{q}\cdot\vec{y}} u^2(\vec{x},\vec{y}) \quad (19a)$$

and

$$F_2(q^2) = -\iiint d^3x d^3y e^{i\frac{2}{3}\vec{q}\cdot\vec{y}} u(\vec{x},\vec{y}) v_1(\vec{x},\vec{y}) , \quad (19b)$$

in terms of configuration space wave functions. In momentum space, they are

$$F_1(q^2) = \iiint d^3\vec{k} d^3\vec{p} u(\vec{k},\vec{p}) u(\vec{k},\vec{p} - \frac{2}{3}\vec{q}) \quad (20a)$$

and

$$F_2(q) = -\iiint d^3\vec{k} d^3\vec{p} u(\vec{k},\vec{p}) v_1(\vec{k},\vec{p} - \frac{2}{3}\vec{q}) . \quad (20b)$$

These latter momentum space expressions were first used to actually calculate  $^3\text{H}$  and  $^3\text{He}$  charge and magnetic moment form factors for realistic nucleon-nucleon force wave functions solutions of the Faddeev equations.<sup>15</sup>

#### IV. Physics of the Trinucleon Form Factors

The form factor is a function of  $q^2$  and not  $q$  even though the exponential argument in Eqs.(16) and (19) is linear in  $\vec{q}$ . Odd powers vanish in the transform because of the isotropic dependence of the charge density upon the direction of the external vector  $\vec{q}$ . For a general density  $\rho(r)/4\pi$ , one obtains

$$F = \frac{1}{4\pi} \int d^3r \rho(r) e^{i\vec{q}\cdot\vec{r}} \quad (21a)$$

$$= \int_0^\infty dr r^2 \rho(r) J_0(qr) \quad (21b)$$

which is clearly even in powers of  $q$ . Expanding Eq.(21b) for small values of  $q$ , one obtains the usual expansion of the form factor in terms of the rms radius  $\langle r^2 \rangle$  of the system:

$$F(q^2) = 1 - \frac{1}{6} \langle r^2 \rangle q^2 \quad (22)$$

where

$$\langle r^2 \rangle = \int_0^\infty dr r^4 \rho(r) \quad (23)$$

and

$$1 = \int_0^\infty dr r^2 \rho(r) . \quad (24)$$

It is clear from Eq.(22) that the larger the size of the system, the faster the form factor falls away from  $F(q^2=0) = 1$ .

Let us apply this result to an analysis of the trinucleons. Martino recently reported values for the rms radii of  $^3\text{He}$  and  $^3\text{H}$  of 1.93(3) fm and 1.81(5) fm respectively.<sup>16</sup> The  $^3\text{He}$  charge density has a radius some 6% larger than that of  $^3\text{H}$ . If all the nucleon-nucleon forces were equal, the two radii would be the same. (See Fig.10a.) They are not. The neutron-proton spin-triplet force is stronger, binding the deuteron, whereas the neutron-proton singlet force, the proton-proton force, and the neutron-neutron force all lead to just unbound singlet states. The charge in  $^3\text{He}$  is carried by the like pair of nucleons; the charge in  $^3\text{H}$  is carried by the odd nucleon. This is illustrated in Figs. 10b and 10c. Because the spin-triplet and spin-singlet forces are not equivalent, the like pair of nucleons is distributed differently from the odd nucleon. In particular, the interaction between like nucleons is weaker than the average neutron-proton interaction, such that the like nucleons lie farther from the centre-of-mass than does the odd nucleon - the like nucleon pair distribution is more extended in space.<sup>12,17</sup> Because the charge radius is the average distance between the protons and the centre-of-mass, the  $^3\text{He}$  charge radius is greater than the  $^3\text{H}$  charge radius. This manifests itself in the wave function through the appearance of the S'-state wave function component. This S'-state of mixed spatial symmetry is a spin(isospin)-space correlation. It is responsible for introducing the  $F_2$  body form factor in Eqs.(15),(17), and (18). It breaks the isoscalar symmetry in the trinucleon charge form factors, introducing an isovector component. Please understand that the difference between  $F_c(^3\text{He})$  and  $F_c(^3\text{H})$  discussed here has absolutely nothing to do with Coulomb repulsion between the two protons in  $^3\text{He}$ . It arises strictly from the spin dependence of the nucleon-nucleon force.

How do Faddeev calculations of the trinucleon wave functions fare with respect to the measured radii? The answer to the question is not simple, because the radius is sensitive to the outer parts of

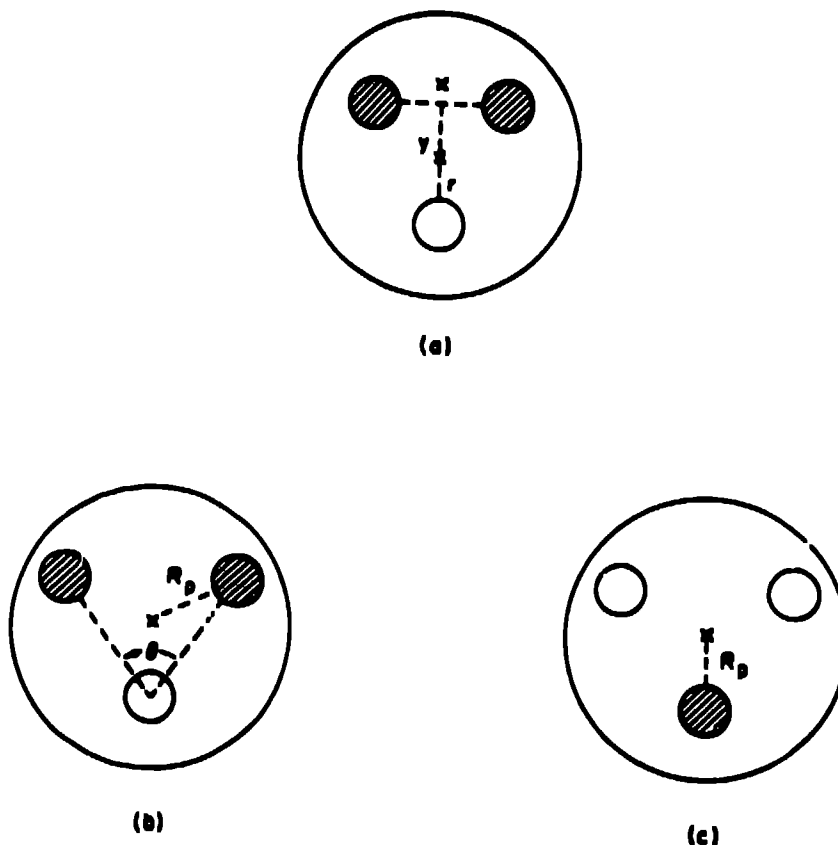


Fig. 10 Schematic model of  ${}^3\text{He}$  with identical forces between protons (shaded) and neutrons in (a).  ${}^3\text{He}$  and  ${}^3\text{H}$  are shown in (b) and (c) when the mn and pp forces are weaker than the average np force.  $R_p$  is the "charge radius".

the wave function which are in turn sensitive to the binding energy  $E_B$  of the system. (The binding energy depends upon the force model selected and the number of channels included in the calculation.) The asymptotic form of the S-state wave function component is proportional to  $\exp(-\kappa\rho)/\rho^{5/2}$  where  $\kappa = (m E_B)^{1/2}$  and  $\rho$  is the usual hyperspherical coordinate ( $\rho^2 = x^2 + y^2$ ). If one assumes that this form is valid over all space, then one obtains<sup>17</sup>

$$\langle r^2 \rangle^{1/2} = 1/(2\kappa) \sim E_B^{-1/2}. \quad (25)$$

This is the binding energy dependence of the isoscalar or mass radius of the  $F_1$  body form factor. In Fig. 11 are shown the results from many calculations of the Los Alamos-Iowa Faddeev group. The symbols refer only to the number of channels and do not indicate whether a two-body or a two-body plus three-body potential model was used. The scaling behavior is clear, although for the  ${}^3\text{He}$  and  ${}^3\text{H}$  charge densities it is more nearly  $E_B^{-1}$  than the  $E_B^{-1/2}$  which holds for the isoscalar radius.<sup>17</sup> Clearly, a model which produces the correct binding energy for the trinucleons will give essentially the correct radii.

How do Faddeev calculations fare for the full form factors, which test more than the asymptotic properties of  $\psi$ ? Except for the

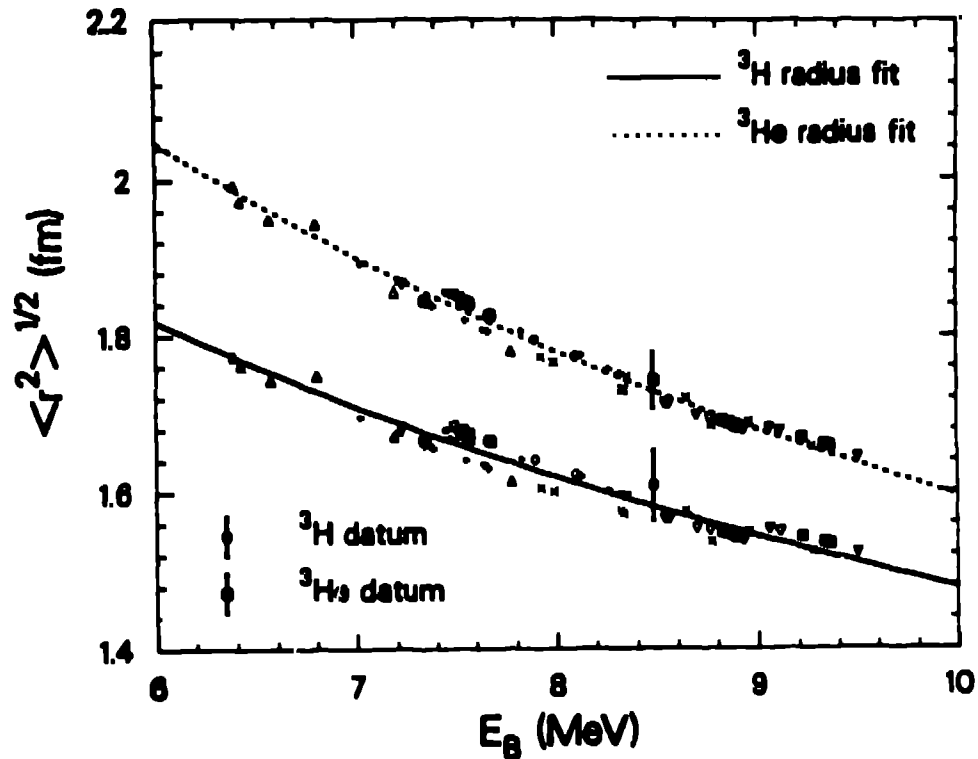


Fig. 11. The  ${}^3\text{He}$  and  ${}^3\text{H}$  rms charge radii plotted versus the triton binding energy  $E_B$  for various model Hamiltonians. The curves are fits to the theoretical values shown.

very-low- $q^2$  region, which is determined essentially by the rms radius of the system, the charge form factor for each of  ${}^3\text{He}$  and  ${}^3\text{H}$  is determined by three numbers in the traditional nuclear physics regime ( $q^2 < 30 \text{ fm}^{-2}$ ).<sup>20</sup> These are the positions of the first diffraction minimum and the secondary diffraction maximum and the value of the form factor at that latter value of  $q^2$ . The most recent Saclay fits<sup>21</sup> to the world's trinucleon form factor data are characterized by

$${}^3\text{He:} \quad q_{\min}^2 = 11.0 \pm 0.7 \text{ fm}^{-2}$$

$$q_{\max}^2 = 15.65 \text{ fm}^{-2}$$

$$F(q_{\max}^2) = - (5.9 \pm 0.3) \times 10^{-3}$$

$${}^3\text{H:} \quad q_{\min}^2 = 12.6 \pm 0.5 \text{ fm}^{-2}$$

$$q_{\max}^2 = 17.25 \text{ fm}^{-2}$$

$$F(q_{\max}^2) = - (3.95 \pm 0.4) \times 10^{-3}.$$

For comparison, results from Ref.20 for these quantities in the case of  $^3\text{H}$  are shown in Figs. 12-14. Nucleon form factors are included. These observables are plotted versus the corresponding binding energy for each model. The triangles, x's, circles, and inverted triangles correspond to the Reid soft core (RSC),<sup>22</sup> Argonne  $V_{14}$  (AV15),<sup>23</sup> super soft core (C) (SSCC),<sup>24</sup> and de Tournell-Rouben-Sprung (B) (TRSB)<sup>25</sup> two-body potential models, respectively. Two-pion-exchange three-nucleon forces [Tucson-Melbourne (TM),<sup>26</sup> Brazilian (BR),<sup>27</sup> and Urbana-Argonne (UA)<sup>28</sup>] were added only to the RSC and AV14 models. All points with  $E_B > 7.7$  MeV contain a three-body force. In each figure there is a band trending upward with increasing binding energy. [Points with small  $E_B$  which lie far off the band correspond primarily to three-channel calculations; they have severely truncated tensor forces and cannot be said to be particularly realistic.] In each case the AV14 model tends to produce larger values of  $q_{\min}^2$  or  $q_{\max}^2$  than the RSC model, and smaller values of  $|F(q_{\max}^2)|$ . A plot for the position of the first diffraction minima in  $^3\text{He}$  is shown in Fig.15 for comparison. The results of these impulse approximation calculations may be summarized as follows: our minima and maxima are at too large a value of  $q^2$  while the values of the maxima are too small, compared with experiment.

This is depicted most clearly in Figs.16 and 17, which compare our RSC 34-channel form factor curves corresponding to three different three-body force models with the experimental data.<sup>21,29-32</sup> The various three-body forces increase the magnitude of the form factor in the region of the secondary maximum but not enough to agree with the data. Moreover, there is a serious problem at more moderate momentum transfers which stems from the fact that the diffraction minima occur at the wrong locations. In the model presented, the fit to the low- $q^2$  data is best without the inclusion of a three-body force.

The ad hoc addition to either form factor of a component which vanishes at  $q^2=0$  and is negative in the region of the diffraction minimum and secondary maximum would alleviate the problems.<sup>20</sup> Such a negative component would shift the form factor minimum and maximum to smaller values of  $q^2$  and would increase the size of the form factor maximum. This simple structural behaviour accounts for the helpfulness of meson-exchange currents. However, we reiterate that there is no fundamental difference between certain pion-exchange contributions to the charge operator and the inclusion of relativistic corrections in the two-nucleon and three-nucleon Hamiltonians ( $\Delta H$ ). The matrix elements of the charge operator have a strength which can be dialed

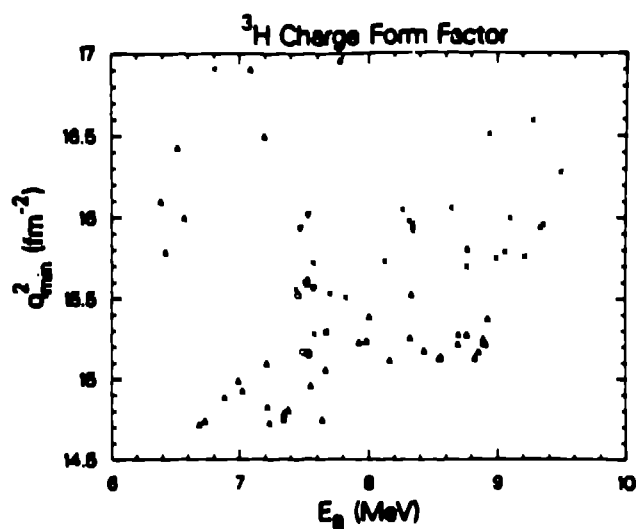


Fig. 12. Position of the first diffraction minimum of the  ${}^3\text{H}$  charge form factor plotted versus the binding energy  $E_B$  for different combinations of the two-body and three-body force models. The triangles, X's, circles, and inverted triangles correspond to the RSC, AV14, SSCC, and TRSB two-body force models.

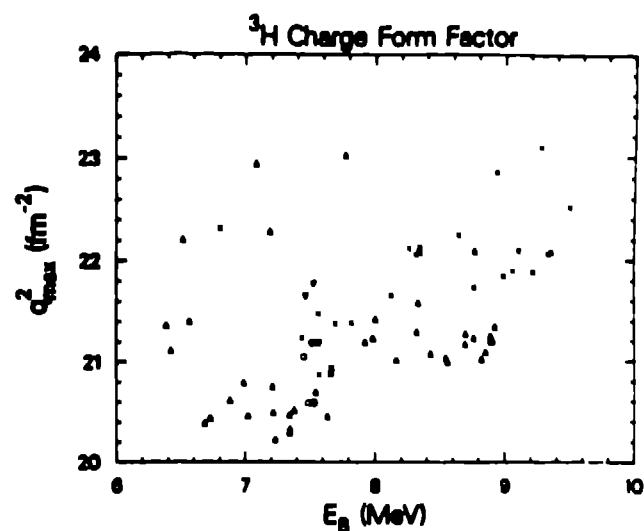


Fig. 13. Position of the secondary diffraction maximum of the  ${}^3\text{H}$  charge form factor plotted versus the binding energy  $E_B$ . The data set and symbols are the same as in Fig. 12.

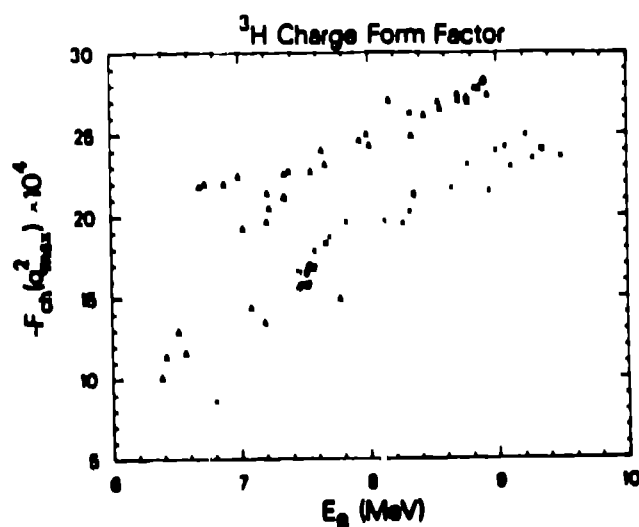


Fig. 14. Magnitude of the secondary diffraction maximum of the  ${}^3\text{H}$  charge form factor plotted versus the binding energy  $E_B$ . The data set and symbols are the same as in Fig. 12.

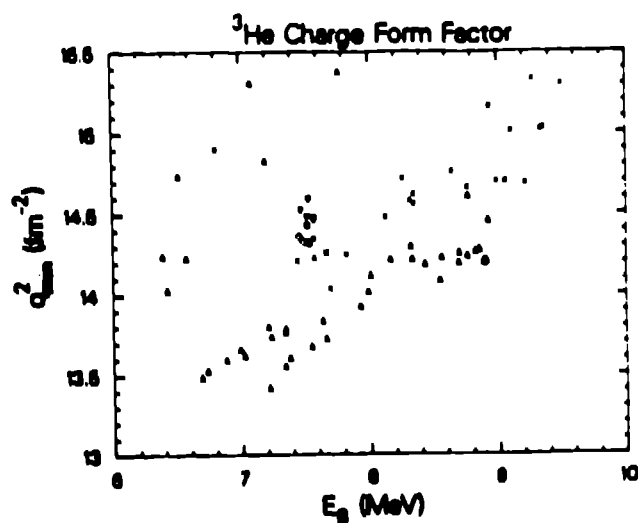


Fig. 15. The  ${}^3\text{He}$  case as in Fig. 12.

from the charge operator into the wave functions via  $\Delta H$  in an arbitrary manner. Those ad hoc calculations of these pion exchange current corrections to the charge operator have heretofore had a negative sign and appropriate strength to alleviate some of the difficulties with fitting the charge form factors.<sup>33</sup> Therefore, it is imperative that trinucleon calculations be performed which include relativistic corrections. [One would prefer a model calculation with the minimal correct physics which avoids the  $(v/c)^2$  expansion.] Only in this way will we be able to make a clear statement about relativistic (and therefore pion exchange current) effects and their role in the trinucleon form factors.

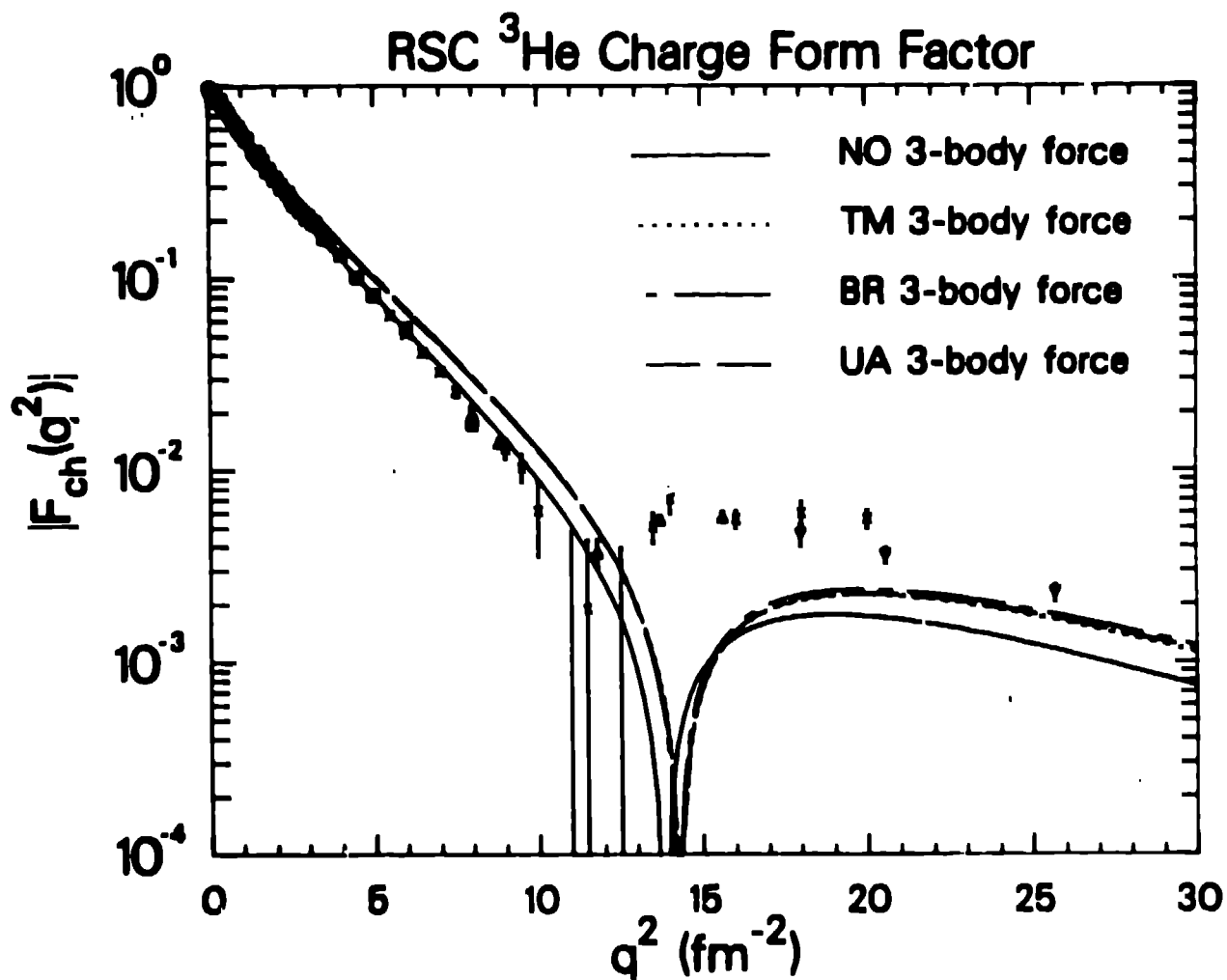


Fig. 16. The magnitude of the RSC  $^3\text{He}$  charge form factor in impulse approximation for several three-body force models plotted versus  $q^2$ , together with the experimental data

What does all of this say about the charge densities of  $^3\text{He}$  and  $^3\text{H}$ ? We plot the point-nucleon impulse approximation charge densities<sup>20</sup> in Figs. 18 and 19. The  $^3\text{He}$  charge density has a maximum at

the origin when no three-body force is included. This is modified to be a slight minimum (except for the TM model) when a three-body force is included. The size of this depression is much smaller than Sick obtained when he Fourier transformed the  $^3\text{He}$  form factor data.<sup>34</sup> This

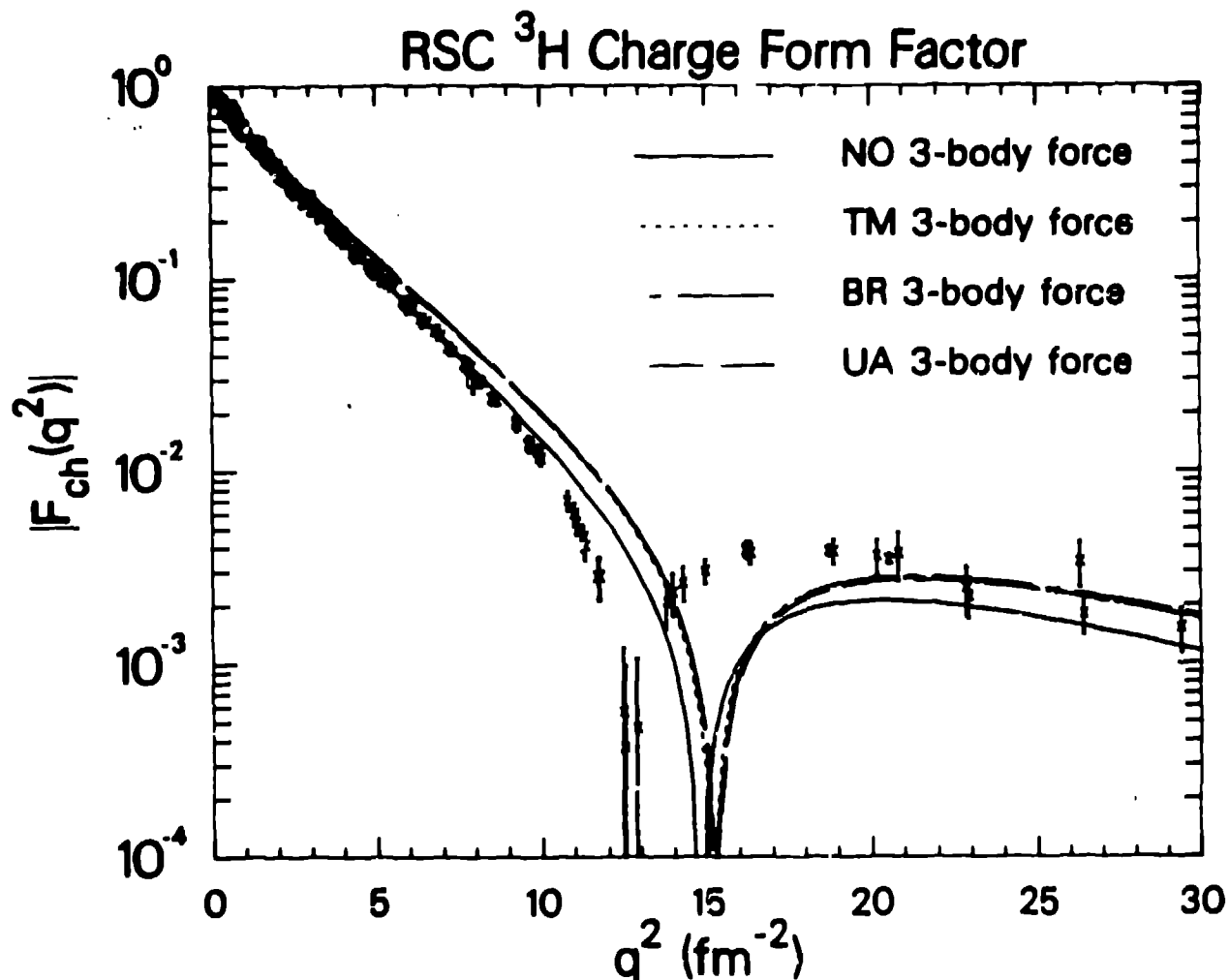


Fig. 17. The magnitude of the RSC  $^3\text{H}$  charge form factor in impulse approximation for several three-body force models plotted versus  $q^2$ , together with the experimental data.

is a reflection of the smaller secondary maximum in the calculated form factors. It is important to realize that the Fourier transform of the experimental form factor is not necessarily properly interpreted as a "charge density." Furthermore, the size of the hole corresponds to less than 1% of the total charge of  $^3\text{He}$ , which is the order of magnitude of relativistic corrections. The difference between the TM curve near the origin and the other three-body force curves reflects the form factor differences at much larger values of  $q^2$  than those shown.

The  $^3\text{H}$  charge density has a small hole for each model. This is caused by the  $L=2$  (D-wave) component of the wave function. This component has a completely symmetric spin-quartet ( $S=3/2$ ) wave func-

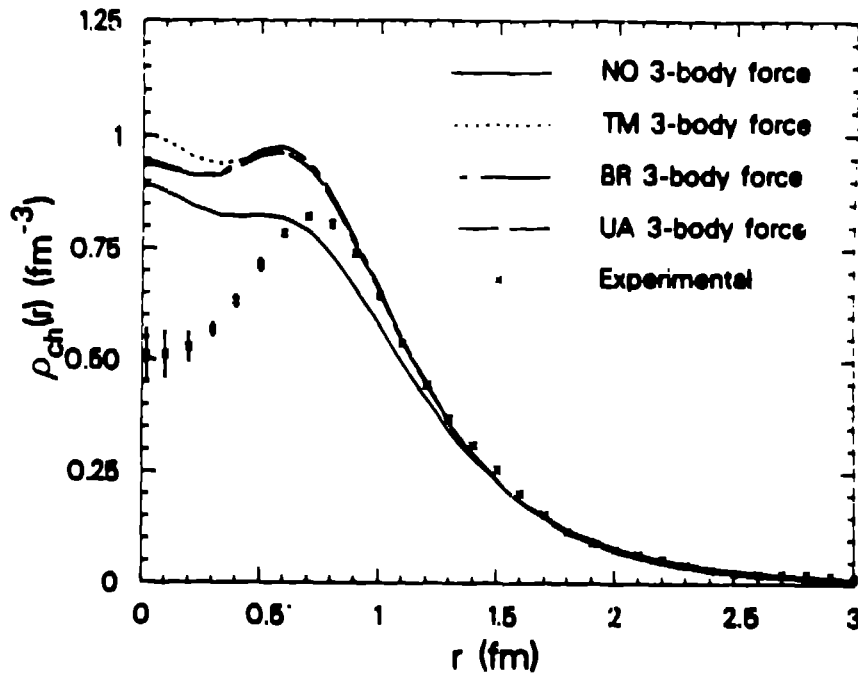


Fig.18. The RSC  ${}^3\text{He}$  charge density in the impulse approximation for several three-body force models plotted versus  $r$ .

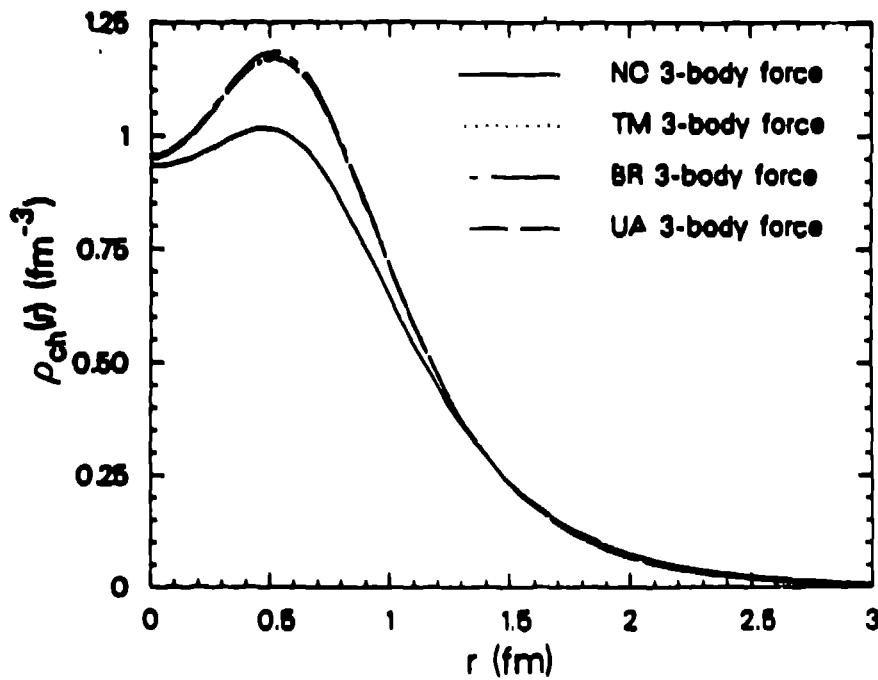


Fig. 19. The RSC  ${}^3\text{H}$  charge density in the impulse approximation for several three-body force models plotted versus  $r$ .

tion. Consequently, the two neutrons in the  $L=2$  component of the triton wave function must be in a relative odd-parity state (to satisfy the Pauli principle) as must be the remaining proton. Therefore, the charge density contribution from this wave function component must vanish at the origin. There is no similar restriction in  ${}^3\text{He}$ , because there are two protons and singling out one of them leaves the remaining neutron-proton pair in any orbital state.

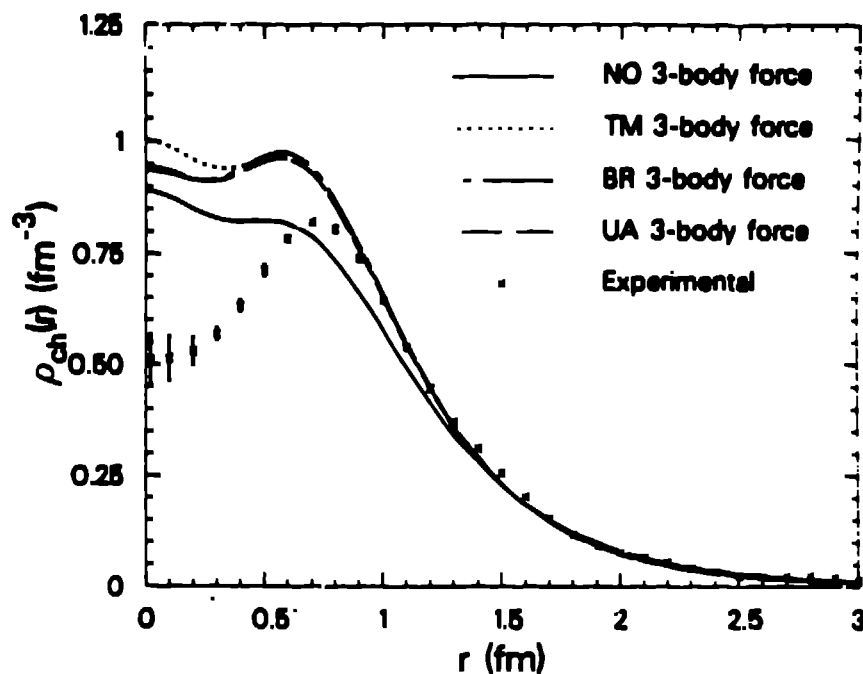


Fig.18. The RSC  ${}^3\text{H}$  charge density in the impulse approximation for several three-body force models plotted versus  $r$ .

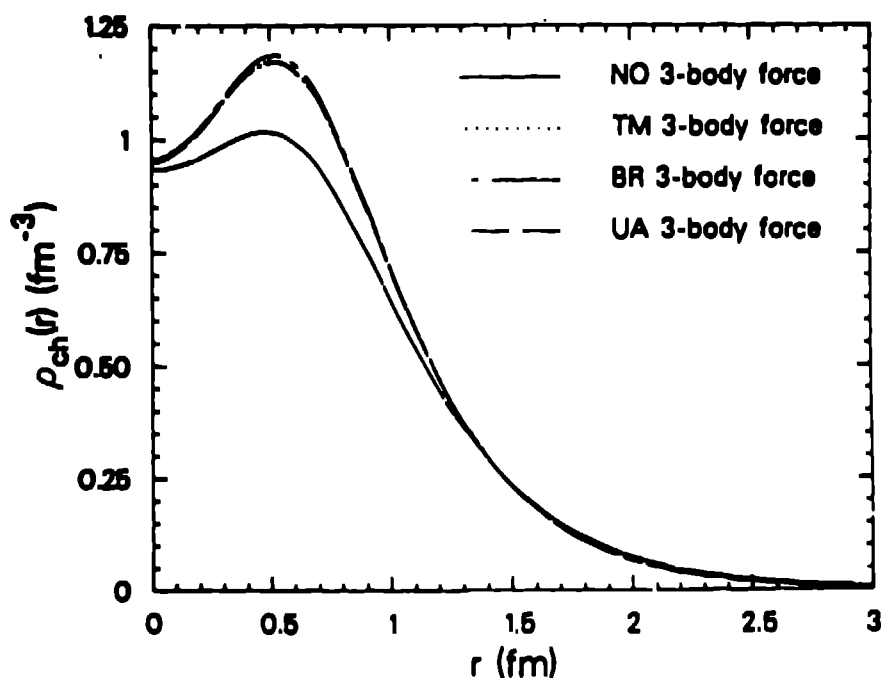


Fig. 19. The RSC  ${}^3\text{H}$  charge density in the impulse approximation for several three-body force models plotted versus  $r$ .

tion. Consequently, the two neutrons in the  $L=2$  component of the triton wave function must be in a relative odd-parity state (to satisfy the Pauli principle) as must be the remaining proton. Therefore, the charge density contribution from this wave function component must vanish at the origin. There is no similar restriction in  ${}^3\text{He}$ , because there are two protons and singling out one of them leaves the remaining neutron-proton pair in any orbital state.

Finally, although it is difficult to observe the effect in Fig. 18 and 19, the increased binding due to the inclusion of a three-body force draws in the charge density toward the origin at large  $r$ . All curves correspond to a normalization of unity.

As a closing note, let us consider the relation between the charge form factors and the Coulomb energy  $E_C$  due to the Coulomb force acting between the two protons in  $^3\text{He}$ . Clearly,  $E_C$  depends upon the size of  $^3\text{He}$  and therefore the binding energy. Friar<sup>35</sup> and Fabre de la Ripelle<sup>36</sup> independently proposed exploiting the hyperspherical approximation, which leads to an estimate ( $E_C^H$ ) for the Coulomb energy in terms of the charge density (and therefore the charge form factor). If one considers the geometrical picture depicted in Fig. 10a, then for an equilateral triangle corresponding to the dominant S-state component of  $\psi$ , the distance  $x$  between the two protons is  $\sqrt{3} r$ . Consequently, for a smooth operator such as  $1/x$ , one obtains as a reasonable approximation

$$E_C^H = E_C, \quad (26)$$

where

$$E_C = \langle \psi | \frac{q}{x} | \psi \rangle \quad (27a)$$

and

$$E_C^H = \frac{1}{\sqrt{3}} \langle \psi | \frac{q}{r} | \psi \rangle. \quad (27b)$$

The idea is to replace the two-body correlation function (required to calculate  $\langle \frac{1}{x} \rangle$ ) by the one-body charge density (needed to evaluate  $\langle \frac{1}{r} \rangle$ ). There is no a priori reason that this must work. If  $\frac{1}{x}$  were instead  $\delta(x)$  and one tried to replace it by  $\delta(r)$ , the approximation would obviously fail badly, as  $\langle \psi | \delta(x) | \psi \rangle = 0$  whereas one can see from Figs. 18 and 19 that  $\langle \psi | \delta(r) | \psi \rangle \neq 0$ . Nevertheless, we have shown by actual calculation that it works remarkably well for the Coulomb energy.<sup>17</sup> This can be seen in Fig. 20, where  $E_C$  is plotted versus  $E_C^H$ . The  $E_C^H$  approximation is less than 1% larger than  $E_C$  for all models. The difference arises because the correlation function is suppressed more than the charge density for small values of their argument when there is short-range repulsion.<sup>37</sup>

The approximation is quite useful because we have available experimental charge form factor data which can be used to calculate  $E_C^H$ . One obtains<sup>38</sup>  $638 \pm 10$  keV for the Coulomb energy of  $^3\text{He}$ . (This is smaller than the 650 keV one would obtain for  $E_B = 8.5$  MeV in model calculations, because the experimental form factors are of larger

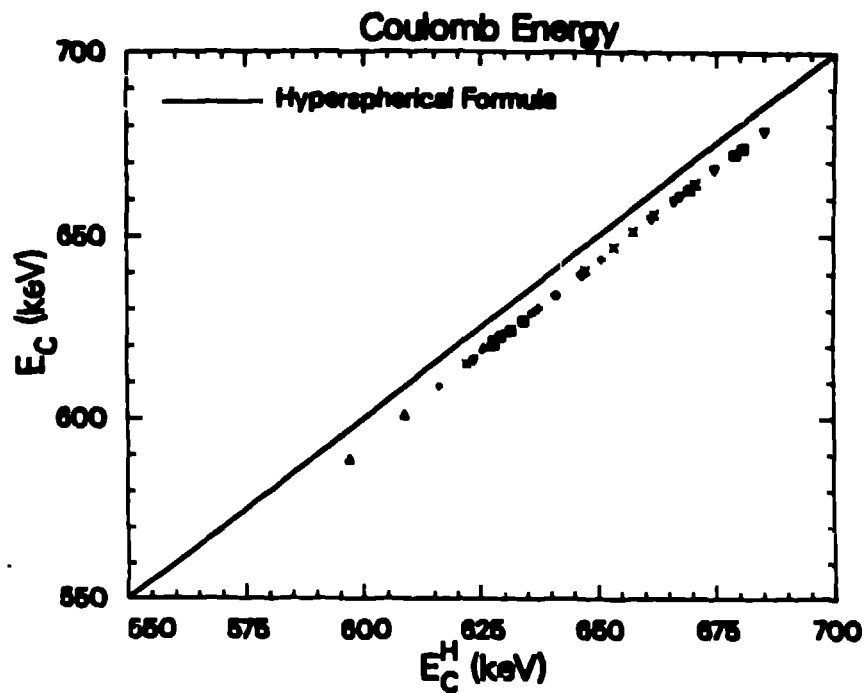


Fig. 20. The  ${}^3\text{He}$  Coulomb energy  $E_C$  plotted versus the hyperspherical approximation.

magnitude in the region of the secondary maximum where they are negative.) The experimental binding energy difference between  ${}^3\text{H}$  and  ${}^3\text{He}$  is 764 keV. The fact that this binding energy difference is larger than the Coulomb energy is a clear indication of the presence of charge symmetry breaking forces in the nuclear Hamiltonian. That is, the neutron-neutron and proton-proton strong interactions are not identical. The known mixing of the  $\rho$  and  $\omega$  and the  $\pi^0$  and  $\eta$  would lead one to predict at least a small charge asymmetry in the nucleon-nucleon force. However, the size of the effect seen here is not fully understood.

## LECTURE II. Two-Body Photodisintegration of the Triton

### I. Introduction

The photon makes an ideal probe of the nucleus. The interaction operator is reasonably well understood. Thus, one may ask questions of the nuclear system independent of the interaction mechanism. We have seen how the virtual photon of electron scattering can be used to study the charge density of the trinucleons. Let us now look at how

the real photon can be used to investigate the principal physics of the  $A=3$  continuum.

Before turning to that problem, I would like to enumerate a few of the interesting aspects of low-energy photonuclear physics, lest you think that trinucleon photodisintegration is the only story. It was only a little more than 50 years ago that the first photonuclear experiment took place:<sup>41</sup>  $^2\text{H} + \gamma \rightarrow n + p$ . The inverse of that reaction (thermal capture of neutrons by hydrogen), with a cross section (of 330 mb) some 10% larger than theoretical models could account for, produced the first incontrovertible evidence for meson exchange current effects in nuclei.<sup>42</sup> The threshold  $n+d \rightarrow ^3\text{H} + \gamma$  reaction has a cross section (of 0.52 mb) some 600 times smaller,<sup>43</sup> and meson exchange current effects are enhanced (to 50%) relative to the standard nucleon current transition.<sup>44</sup> By exploring such processes in which normally dominant reaction mechanisms are suppressed, one can investigate details of nuclear physics which would otherwise be difficult to see. Another example is the forward ( $0^\circ$ ) photodisintegration of deuterium.<sup>45</sup> Because the normally dominant E1

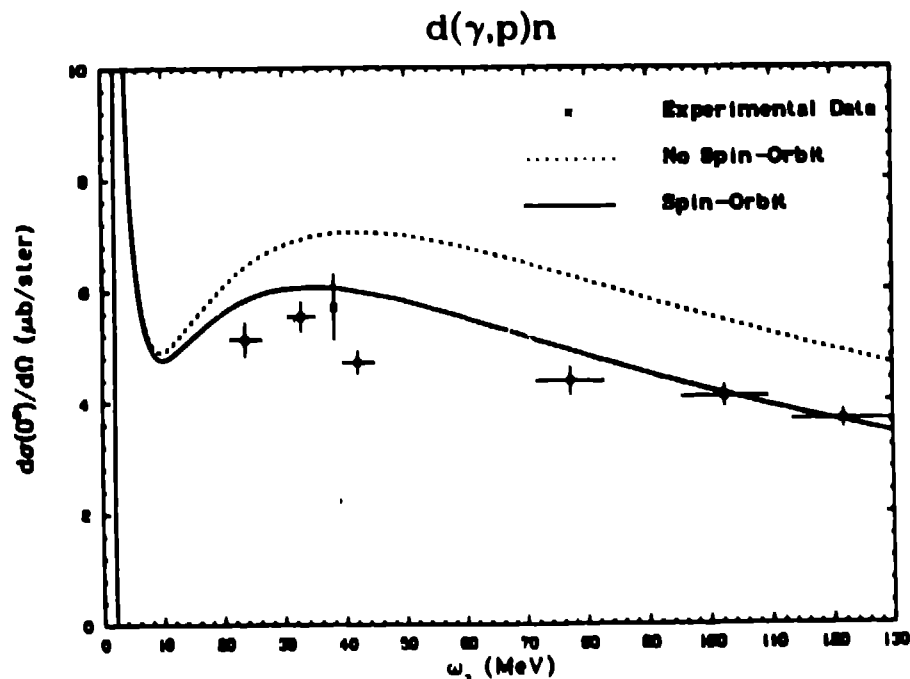


Fig. 21. Model calculations of the  $^2\text{H}(\gamma, p)n$  reaction at  $0^\circ$  with and without the relativistic spin-orbit contribution to the E1 operator. The data are from Ref. 45.

transition from the  $L=0$  component of the initial state to the  $L=1$  partial wave of the final state vanishes in this geometry, one can clearly observe noncentral force effects.<sup>46</sup> In particular, the spin orbit terms provide a 20% enhancement of  $d\sigma/d\Omega$  for  $\theta=0^\circ$  as can be seen in Fig. 21. I will not have time to discuss the 85%-90% suppression of the  $T=1/2$  channel in the three-body photodisintegration of  $^3\text{H}$  and  $^3\text{He}$ , compared to the  $T=3/2$  channel.<sup>47-50</sup> It is, however, intimately related by three-body unitarity to the two-body breakup channel. Finally, one of the long standing puzzles in nuclear physics is the deviation from 1 of the ratio of photoneutrons and photocoprotons from an alpha particle; i.e., experimentally one finds (see Fig. 22)

$$\sigma[^4\text{He}(\gamma, p)^3\text{H}] / \sigma[^4\text{He}(\gamma, n)^3\text{He}] \neq 1$$

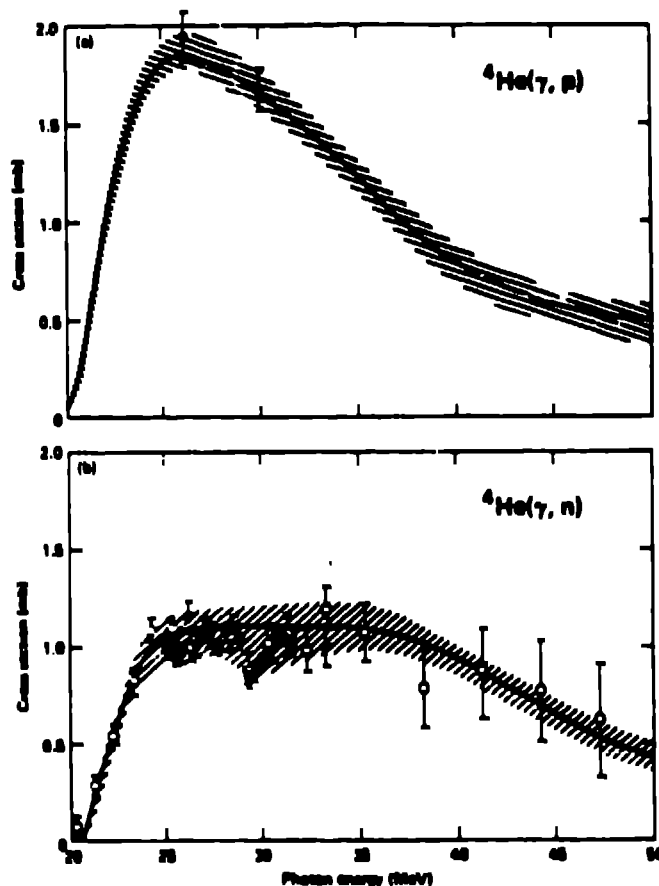


Fig. 22. The  $^4\text{He}(\gamma, p)^3\text{H}$  and  $^4\text{He}(\gamma, n)^3\text{He}$  cross section evaluation (solid line); data in (a) are from Ref. 51

for  $E_\gamma < 30$  MeV, in contradiction to that which one would expect on the basis of simple charge symmetry arguments.<sup>52</sup> The list goes on.

In addition to the fact that few-body photonuclear reactions yield interesting physics, there are purely theoretical reasons for attempting to model these reactions.<sup>50</sup> At low energy only a few multipoles are important. That is not to say that higher multipoles

can necessarily be neglected, but they can be treated adequately in Born approximation. As a consequence, large partial wave sums do not hide the physics. One can methodically examine a reaction and come to an understanding of the physics; e.g. the  $0^+$  photodisintegration of deuterium. Because only a few multipoles and partial waves dominate the problem, "exact" model calculations are not impossibly long. Thus, photonuclear reactions are an appropriate field in which to study the application of exact equation techniques in nuclear physics.

We shall examine below, as our example, the electric dipole (E1) two-body photodisintegration of tritium:



We employ a separable potential formalism and restrict our consideration to central forces. This model has been investigated thoroughly by Barbour and Phillips<sup>48</sup> and independently by Gibson and Lehman<sup>53</sup> using a description of the nd off-shell scattering that resembles closely the formalism of Alt, Grassberger, and Sandhas.<sup>54</sup> The E2 contribution was shown to be negligible for photon energies of less than 40 MeV by Barbour and Hendry.<sup>55</sup> The physics points of interest are (1) the cross section calculation does depend on whether the initial and final states are eigenfunctions of the same Hamiltonian, (2) the full calculation is 50% larger than the plane-wave Born approximation result at the peak of the  $90^\circ$  differential cross section, and (3) the enhancement is due to using exact equations which incorporate proper three-body unitarity and therefore couple the two-body (nd) breakup channel to the  $T=1/2$  three-body breakup (nnp) channel.<sup>53</sup>

## II. The E1 operator

For those not familiar with photonuclear reactions, the matrix elements of the multipole series are known to go like  $EL \sim (kR)^L$  at low energy, where  $k$  is the photon momentum (energy) in  $\text{fm}^{-1}$  and  $R$  is the size of the nuclear system of interest. We have seen that the trinucleon radius is less than 2 fm. A photon of 20 MeV energy has  $k \approx 0.1 \text{ fm}^{-1}$ . Thus the ratio of E2 to E1 matrix elements is  $\sim 0.1$ , and the E1 operator dominates the low-energy photodisintegration reaction.

Recall that the charge density operator relevant to the calculation of charge form factors is of the form

$$\rho(x_1) = e\delta(\vec{x} - \vec{x}_1) \frac{1}{2} (1 + \tau_{12}) \quad (28)$$

for a point charge. Meson exchange current contributions to the charge density operator are  $(v/c)^2$  relativistic corrections. What do we find for the E1 photodisintegration operator?

Formally, we wish to investigate the Hamiltonian

$$H_{\text{Total}} = H + H' , \quad (29)$$

where  $H'$  is the interaction which will be treated perturbatively and  $H$  is the nuclear Hamiltonian composed of kinetic energy and pair interactions. That is, we assume

$$H = H_0 + V \quad (30)$$

where the initial- and final-state eigenfunctions satisfy

$$H|\psi_i\rangle = E_i|\psi_i\rangle \quad (31a)$$

and

$$H|\psi_f\rangle = E_f|\psi_f\rangle . \quad (31b)$$

The matrix element  $M_{if}$  which determines the transition from  $\psi_i$  to  $\psi_f$  is then given by

$$M_{if} = \langle \psi_f | H' | \psi_i \rangle . \quad (32)$$

The cross section for the reaction is

$$\sigma = \int \sum_{if} |M_{if}|^2 df, \quad (33)$$

where  $\sum_{if}$  is the sum over final spin states and average over initial spin states and  $\int df$  is the required phase space integral.

The transition matrix element involves the interaction of the photon field  $\hat{\epsilon} \exp(i\vec{k} \cdot \vec{r})$ , where  $\hat{\epsilon}$  is the photon polarization and  $\vec{k}$  its momentum vector ( $\hat{\epsilon} \cdot \vec{k} = 0$ ), with the nuclear current  $\vec{J}$ . The current  $\vec{J}$  consists of a nucleon component and a meson exchange component:

$$\vec{J} = \vec{J}_N + \vec{J}_{\text{MEC}} . \quad (34)$$

The nucleon current has the expected form

$$\mathbf{J}_N(\mathbf{x}_1) = \frac{e}{2m} \{ \mathbf{p}_1, \delta(\mathbf{x} - \mathbf{x}_1) \} . \quad (35)$$

That is, it is proportional to  $\mathbf{p}/m$ , the velocity of the nucleon. Note that it is of order  $(v/c)$ , whereas the charge density is  $(v/c)^0$  and its exchange current corrections are  $(v/c)^2$ . Unfortunately, meson exchange current corrections to  $\mathbf{J}$  are also of order  $(v/c)$  and cannot, therefore, be neglected. However, it was pointed out by Siegert<sup>56</sup> in the late 1930's that one can include the principal effects of meson exchange currents in the long wave length limit (i.e. the low-energy region in which we are interested) by making use of the charge continuity equation

$$\nabla \cdot \mathbf{J} = - \frac{d}{dt} \rho = -i[\rho, H] . \quad (36)$$

Long wave length limit means to lowest order in  $\mathbf{k}$ . In a nucleons-only regime, where  $J_{MEC} = 0$ , the electric dipole current is

$$\mathbf{J} \sim \mathbf{p}/m = \dot{\mathbf{r}} = i[\mathbf{r}, H] . \quad (37)$$

In that case, the transition matrix element becomes

$$M_{if} = i \langle \psi_f | \dot{\mathbf{r}} \cdot [\mathbf{r}, H] | \psi_i \rangle \quad (38a)$$

$$= i(E_f - E_i) \langle \psi_f | \dot{\mathbf{r}} \cdot \mathbf{r} | \psi_i \rangle . \quad (38b)$$

Thus, the long wave length limit form of the electric dipole operator is  $\dot{\mathbf{r}} \cdot \mathbf{r}$ . The same result is achieved when the general current  $\mathbf{J}$  is used by writing

$$\dot{\mathbf{r}} \cdot e^{i\mathbf{k} \cdot \mathbf{r}} = \int_0^1 ds \{ \nabla \cdot [\dot{\mathbf{r}} \cdot \mathbf{r} e^{is\mathbf{k} \cdot \mathbf{r}}] - i s \mathbf{r} \times [\mathbf{k} \times \dot{\mathbf{r}}] e^{is\mathbf{k} \cdot \mathbf{r}} \} . \quad (39)$$

The second term generates magnetic multipoles, so that we concentrate on the first. Thus, we consider

$$M_{if} = \langle \psi_f | \int_0^1 ds \mathbf{J} \cdot \nabla [\dot{\mathbf{r}} \cdot \mathbf{r} e^{is\mathbf{k} \cdot \mathbf{r}}] | \psi_i \rangle . \quad (40)$$

Performing an integration by parts and utilizing the current conservation relation to replace the  $\nabla \cdot \mathbf{J}$  operation with the commutator of a point nucleon charge density and  $H$ , we obtain

$$M_{if} = i \langle \psi_f | \int_0^1 ds \, \vec{\epsilon} \cdot \vec{r} \, e^{is\vec{k} \cdot \vec{r}} | \psi_i \rangle . \quad (41)$$

Again, because the initial and final states are eigenfunctions of  $H$ , we can evaluate the commutator and perform the  $\int ds$  to obtain

$$M_{if} = (E_f - E_i) \sum_L (i)^L \langle \psi_f | \vec{\epsilon} \cdot \vec{r} \frac{(\vec{k} \cdot \vec{r})^{L-1}}{L!} | \psi_i \rangle , \quad (42)$$

the leading term of which is

$$M_{if} = i\omega \langle \psi_f | \vec{\epsilon} \cdot \vec{r} | \psi_i \rangle , \quad (43)$$

where  $\omega = E_f - E_i = |\vec{k}|$ . Thus, the Siegert (long wave length) limit of the electric dipole operator which includes the meson exchange current as well as the nucleon current ( $\vec{p}/m$ ) is  $\vec{\epsilon} \cdot \vec{r}$ .

Let me conclude this discussion by pointing out that there is an additional reason for using the Siegert form of the transition operator when one is forced to use approximate solutions to the nuclear Hamiltonian. Because the Siegert operator is related to the charge density, we are able to enforce some physical intuition in normalizing the bound-state spatial density; the normalization for the current density of the nucleus is unknown. Furthermore, care should be exercised to avoid the temptation to use the current form of the operator even when exact eigenstates of the nuclear Hamiltonian exist, as they do for the separable potential model. The requirement of gauge invariance introduces a gauge transformation in all nonlocal, momentum-dependent potentials when  $\vec{\epsilon} \cdot \vec{p}$  is used. This complexity (see Yamaguchi<sup>57</sup> for a discussion of  $^2\text{H}$  photodisintegration) is avoided by use of the Siegert forms of the E1 and E2 operators  $\vec{\epsilon} \cdot \vec{r}$  and  $\frac{1}{2} (\vec{\epsilon} \cdot \vec{r})(\vec{k} \cdot \vec{r})$ ; the appropriate meson exchange currents are properly included.

### III. Separable Potential Formalism

The nuclear Hamiltonian is assumed to be of the form given in Eq.(30), when the potential operator is

$$V = \sum_{a=1}^3 V_a \equiv V_{23} + V_{31} + V_{12} . \quad (44)$$

The eigenstates of  $H$  are assumed to be those corresponding to a three-body bound state, a scattering state comprised of a nucleon plus a bound pair, and a scattering state of three unbound nucleons. Thus we

have

$$H|\psi_B\rangle = -E_B|\psi_B\rangle, \quad E_B > 0; \quad (45)$$

$$H|\psi_{an\vec{p}}\rangle = E_{an}^{(2)}|\psi_{an\vec{p}}\rangle, \quad E_{an}^{(2)} = \frac{p^2}{2m_a} - \epsilon_{an}, \quad \epsilon_{an} > 0; \quad (46)$$

$$H|\psi_{an\vec{p}\vec{k}}\rangle = E_{an}^{(3)}|\psi_{an\vec{p}\vec{k}}\rangle, \quad E_{an}^{(3)} = \frac{p^2}{2m_a} + \frac{k^2}{2\mu_a}. \quad (47)$$

The reduced masses are  $m_a = M_a(M_\beta + M_\gamma)/\Sigma M_a$  and  $\mu_a = M_\beta M_\gamma/(M_\beta + M_\gamma)$ , where  $M_a$  is the mass of particle  $a$ . For three equal mass nucleons, these reduce to  $2M/3$  and  $M/2$ , respectively. The subscripts in Eq.(47) mean that nucleon  $a$  moves relative to the center-of-mass of the pair  $\beta\gamma$  with momentum  $\vec{p}$ , while  $\beta$  and  $\gamma$  move relative to each other with momentum  $\vec{k}$ . The subscript  $n$  in Eqs.(46) and (47) denotes the remaining quantum numbers such as spin and isospin.

We are concerned here only with two-body photodisintegration, which is described by the transition amplitude matrix element

$$A_2(\alpha, n, \vec{p}) = \langle \psi_{an\vec{p}}^{(-)} | H' | \psi_B \rangle, \quad (48)$$

where the superscript  $(-)$  denotes the outgoing state which corresponds asymptotically to an incoming wave boundary condition. The two-body scattering state is a solution of the equivalent equations

$$(n > 0; E = p^2/2m_a - \epsilon_{an})$$

$$|\psi_{an\vec{p}}^{(-)}\rangle = |\phi_{an\vec{p}}\rangle - G_a(E-i\eta) \sum_{\beta \neq a} V_\beta |\psi_{an\vec{p}}^{(-)}\rangle \quad (49)$$

and

$$|\psi_{an\vec{p}}^{(-)}\rangle = |\phi_{an\vec{p}}\rangle - G(E-i\eta) \sum_{\beta \neq a} V_\beta |\phi_{an\vec{p}}\rangle, \quad (50)$$

with the resolvent operators defined as

$$G_a(z) = [H_0 + V_a - z]^{-1} \quad (51)$$

and

$$G(z) = [H - z]^{-1}. \quad (52)$$

The  $|\phi_{an\vec{p}}\rangle$  denotes the asymptotic scattering state comprised of a nucleon  $a$  moving freely with respect to the  $\beta\gamma$  bound pair. In Eq.(50)

is written in terms of the distortion operator

$$\bar{\Omega}_\alpha^{(-)} \equiv \bar{\Omega}_\alpha(E-i\eta) = 1 - G(E-i\eta) \sum_{\beta \neq \alpha} V_\beta \quad (53)$$

and substituted into Eq.(48), we obtain

$$A^2(\alpha, n, \vec{p}) = \langle \phi_{\alpha n \vec{p}} | \Omega_\alpha^{(+)} H' | \psi_B \rangle, \quad (54)$$

where  $\Omega_\alpha^{(+)} = (\bar{\Omega}_\alpha^{(-)})^\dagger$ . The crux of this operator manipulation is that a Faddeev-like equation can be written for  $\Omega_\alpha^{(+)}$ :

$$\Omega_\alpha^{(+)} = (\bar{\Omega}_\alpha^{(-)})^\dagger = 1 - \sum_{\beta \neq \alpha} V_\beta G(E+i\eta) = G_\alpha^{-1}(E+i\eta) G(E+i\eta) \quad (55a)$$

$$= 1 - \sum_{\beta \neq \alpha} V_\beta G_\beta G_\beta^{-1} G \quad (55b)$$

$$= 1 - \sum_{\beta \neq \alpha} V_\beta G_\beta \Omega_\beta^{(+)}, \quad (55c)$$

Equation (55c) can then be reexpressed in terms of the two-body  $t$ -matrix operator as

$$\Omega_\alpha^{(+)} = 1 - \sum_{\beta=1}^3 \tilde{\tau}_{\alpha\beta} T_\beta G_0 \Omega_\beta^{(+)}, \quad (56)$$

because

$$T_\beta(z) G_0(z) = V_\beta G_\beta(z), \quad (57)$$

where  $\tilde{\tau}_{\alpha\beta} = 1 - \delta_{\alpha\beta}$  and  $G_0(z) = (H_0 - z)^{-1}$ . If one then iterates Eq.(56) to obtain

$$\Omega_\alpha^{(+)} = 1 - \sum_{\beta=1}^3 \tilde{\tau}_{\alpha\beta} T_\beta G_0 + \sum_{\beta=1}^3 \sum_{\gamma=1}^3 \tilde{\tau}_{\alpha\beta} T_\beta G_0 \tilde{\tau}_{\beta\gamma} T_\gamma G_0 - + \dots \quad (58)$$

and regroups terms as

$$\Omega_\alpha^{(+)} = 1 - \sum_{\gamma=1}^3 (\tilde{\tau}_{\alpha\gamma} - \sum_{\beta=1}^3 \delta_{\alpha\beta} T_\beta G_0 \delta_{\beta\gamma} + \dots) T_\gamma G_0, \quad (59)$$

then it is possible to recognize the expression in parenthesis in Eq.(59) as  $G_0^{-1} X_{\alpha\gamma}$ , where  $X_{\alpha\gamma}$  is the transition operator that connects particle-plus-correlated-pair states. Therefore, one can write

$$\Omega_\alpha^{(+)} = 1 - \sum_{\gamma=1}^3 G_0^{-1} X_{\alpha\gamma} T_\gamma G_0, \quad (60)$$

where

$$X_{\alpha\beta}(z) = G_0(z)\delta_{\alpha\beta} - \sum_Y X_{\alpha Y}(z)T_Y(z)\delta_{Y\beta}G_0(z) \quad (61a)$$

or

$$X_{\alpha\beta}(z) = G_0(z)\delta_{\alpha\beta} - G_0(z) \sum_Y \delta_{\alpha Y}T_Y(z)X_{Y\beta}(z) . \quad (61b)$$

The three-body dynamics of the continuum state now reside in the transition operator  $X_{\alpha Y}$ . The two-body photodisintegration amplitude can be written as

$$A^2(\alpha, n, \vec{p}) = \langle \phi_{\alpha n \vec{p}} | H' | \psi_B \rangle - \sum_{Y=1}^3 \langle \phi_{\alpha n \vec{p}} | G_0^{-1}(z) X_{\alpha Y}(z) T_Y(z) G_0(z) H' | \psi_B \rangle , \quad (62)$$

where  $z = p^2/2m\alpha - \epsilon_{\alpha n} + i\eta$ , and the three-body dynamics and the photodisintegration operator have been separated.

The application of Eq.(62) to the photodisintegration of  $^3\text{H}$  requires knowledge of both  $T_\alpha(z)$  and  $H'$ . For this illustration, we assume that  $T_\alpha(z)$  results from an attractive, central-force, spin-dependent interaction<sup>57</sup>

$$v_n(k, k') = - \frac{\lambda_n}{2\mu} g_n(k) g_n(k') , \quad (63)$$

where the  $\lambda_n$  are the strengths of the interactions and

$$g_n(k) = \langle \vec{k} | g_n \rangle$$

are the momentum dependent form factors which determine the ranges of the interactions. This separable form of the nucleon-nucleon interaction can support a bound state, and we will assume that the spin-triplet (t) potential does but that the spin-singlet (s) potential does not. The deuteron bound-state wave function is

$$\langle \chi_t | = N_2 \langle g_n | G_0^{(2)}(-\epsilon_t) , \epsilon_t > 0 , \quad (64)$$

where  $N_2$  is the normalization constant chosen so that  $\langle \chi_t | \chi_t \rangle = 1$  and  $G_0^{(2)}(z)$  is the free-particle resolvent for two nucleons [in contrast to  $G_0(z)$  which is the free-particle resolvent for three nucleons]. In this picture we have

$$T_{\alpha}(z) = - \sum_{n=s}^{\infty} |g_{\alpha n}\rangle \tau_{\alpha n}(z) \langle g_{\alpha n}| (|S\rangle \langle SI|)_{\alpha n} ,$$

where

$$\tau_{\alpha n}(z) = \frac{\lambda_n}{2\mu_{\alpha}} \left( 1 + \frac{\lambda_n}{2\mu_{\alpha}} \int d^3k \frac{g_n^2(k)}{z - k^2/2\mu_{\alpha}} \right)^{-1} . \quad (66)$$

The upper case  $S(I)$  denote the total spin (isospin) wave functions for three nucleons. (See Appendix B for details.) Our asymptotic continuum state becomes

$$\langle \phi_{\alpha n \vec{p}} | = N_2 \langle g_{\alpha n} \vec{p} | G_0 \left( \frac{p^2}{2m_{\alpha}} - \epsilon_{\alpha n} \right) \quad (67)$$

with  $\langle g_{\alpha n} \vec{p} | = \langle g_{\alpha n} | \langle \vec{p} |$ , and we can write Eq.(62) as

$$\begin{aligned} A^2(\alpha, n, \vec{p}) = & N_2 \{ \langle g_{\alpha n} \vec{p} | G_0(z) H' | \psi_B \rangle \\ & + \sum_{\beta=1}^3 \sum_{n'=s}^{\infty} \int d^3p' \langle g_{\alpha n} \vec{p} | X_{\alpha\beta}(z) | g_{\beta n'} \vec{p}' \rangle \tau_{\beta n'} \left( z - \frac{p'^2}{2m_{\beta}} \right) \\ & \times \langle g_{\beta n'} \vec{p}' | G_0(z) H' | \psi_B \rangle \} \end{aligned} \quad (68)$$

where we have suppressed the spin-isospin projection operator in the second term of the expression and used the identity  $\int d^3p' |p'\rangle \langle p'| = 1$ .

For three identical nucleons, one must symmetrize the amplitude:

$$M_2^n(z, \vec{p}) = \sqrt{\frac{1}{3}} \sum_{\alpha=1}^3 A_2(\alpha, n, \vec{p}) . \quad (69)$$

The resulting symmetrized expression can be written as

$$\begin{aligned} M_2^n(z, \vec{p}) = & B_n(z, \vec{p}) \\ & + \sum_{n'=s}^{\infty} \int d^3p' \langle \vec{p} | X_{nn'}(z) | p' \rangle \tau_{n'} \left( z - \frac{3p'^2}{4M} \right) B_{n'}(z, \vec{p}') . \end{aligned} \quad (70)$$

where  $z = 3p^2/4M - \epsilon_d + i\eta$  and the deuteron binding energy  $\epsilon_d = \gamma^2/M = 2.225$  MeV. The amplitudes appearing in Eq.(70), written in off-shell form ( $z$  not equal to  $3p^2/4M - \epsilon_d + i\eta$  and  $|\vec{p}|$  not the

same as  $|\vec{p}'\rangle$ , are

$$B_n(z, \vec{p}) = N_2 \sqrt{\frac{T}{3}} \sum_{\alpha=1}^3 \langle g_{\alpha n} \vec{p} | G_0(z) H' | \Psi_B \rangle \quad (71)$$

and

$$\langle \vec{p} | X_{nn'}(z) | \vec{p}' \rangle = \frac{1}{3} \sum_{\alpha=1}^3 \sum_{\beta=1}^3 \langle g_{\alpha n} \vec{p} | X_{\alpha\beta}(z) | g_{\beta n'} \vec{p}' \rangle. \quad (72)$$

The off-shell three-particle transition amplitude  $\langle \vec{p} | X_{nn'}(z) | \vec{p}' \rangle$  satisfies the integral equation

$$\begin{aligned} \langle \vec{p} | X_{nn'}(z) | \vec{p}' \rangle &= \langle \vec{p} | Z_{nn'}(z) | \vec{p}' \rangle \\ &+ \sum_{m=s}^t \int d^3 p'' \langle \vec{p} | X_{nm}(z) | \vec{p}'' \rangle \tau_m(z - \frac{3p''^2}{4M}) \langle \vec{p}'' | Z_{mn'}(z) | \vec{p}' \rangle, \end{aligned} \quad (73)$$

where

$$\langle \vec{p} | Z_{nn'}(z) | \vec{p}' \rangle = \frac{1}{3} \sum_{\alpha=1}^3 \sum_{\beta=1}^3 \tilde{\tau}_{\alpha\beta} \langle g_{\alpha n} \vec{p} | G_C(z) | g_{\beta n'} \vec{p}' \rangle. \quad (74)$$

The calculational method to be used to obtain the two-body disintegration matrix element is now clear on the basis of Eqs.(70) and (73). For those who prefer a graphical representation, a vivid description is given in Fig.23. The  $X_{nn'}$  amplitudes are obtained by solving the coupled integral equations driven by the one-nucleon exchange term  $Z_{nn'}$ . The matrix describing the two-body photodisintegration is obtained as an integral relation involving these off-shell amplitudes and the Born terms for the disintegration process. It should be noted that one can treat any weak process by this method, since the perturbative operator  $H'$  has not yet been specified.

Taking for our ansatz the electric dipole operator, we have

$$H' = \frac{1}{2} e \sum_i \vec{e} \cdot \vec{r}_i \tau_{iz} \quad (75)$$

where  $r_i$  are the nucleon center-of-mass coordinates and  $\tau_{iz}$  is the z-component isospin Pauli operator for nucleon  $i$ . We include only the dominant S-state component of the triton ground state for this example (see Appendix B):

$$|\Psi_B\rangle = u \bar{\phi}_a, \quad (76)$$

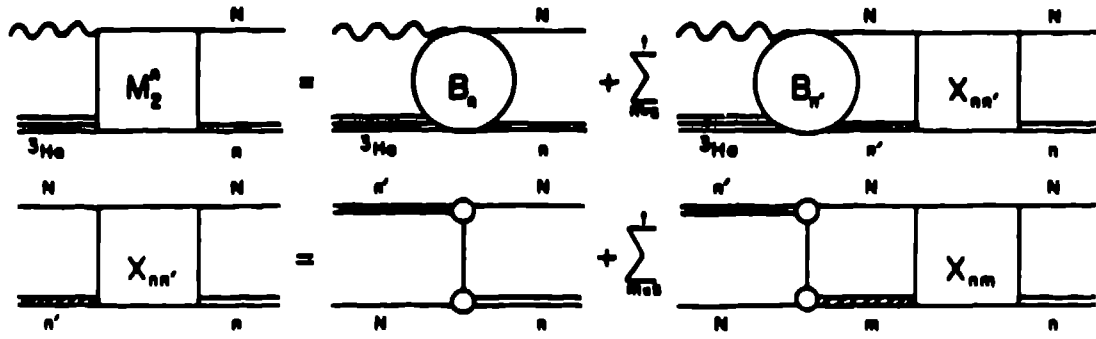


Fig. 23. A graphical representation of the equations used to generate the two-body photodisintegration transition amplitude. The wavy line represents the photon, the double line (n) the deuteron, and N is a neutron in the case of  ${}^3\text{H}$  photodisintegration. The cross-hatched double line indicates that a particular correlated pair plus nucleon are off shell.

where the bar in  $\bar{\phi}_a$  denotes  ${}^3\text{H}$  instead of  ${}^3\text{He}$ . Acting with the operator  $H'$  on  $\psi_B$ , we obtain

$$H'|\psi_B\rangle = \frac{e}{2\sqrt{3}} \vec{\epsilon} \cdot \left[ \frac{2}{\sqrt{3}} \vec{y} \bar{\phi}_2 + \vec{x} \bar{\phi}_1 \right] u(\vec{k}, \vec{p}). \quad (77)$$

The final-state spin-isospin projection in Eq.(71) involves only  $\chi_1 \bar{\eta}_2$  and, because the deuteron wave function is S-wave, we get

$$B_L(z, \vec{p}) = \frac{eMN_2}{\sqrt{6}} \int d^3k \frac{g_L(k) [\vec{\epsilon} \cdot \vec{y} u(\vec{k}, \vec{p})]}{3p^2/4 + k^2 - Mz} \quad (78)$$

where  $\vec{y} = -i\vec{\nabla}_p$ . In the model in which we are working, the electric-dipole operator connects the  ${}^2S_{1/2}$  ground state to the  ${}^2P_{1/2}$  continuum state.

Let us specialize the equations to a calculable form by making partial-wave decompositions:

$$B_n(z, \vec{p}) = \vec{\epsilon} \cdot \vec{p} \mathcal{B}_n(z, p), \quad (79a)$$

$$\langle \vec{p} | X_{nn'} | \vec{p}' \rangle = \sum_L (2L+1) X_{nn'}^L(p, p'; z) P_L(\hat{p} \cdot \hat{p}'), \quad (79b)$$

$$\langle \vec{p} | Z_{nn'} | \vec{p}' \rangle = \sum_L (2L+1) Z_{nn'}^L(p, p'; z) P_L(\hat{p} \cdot \hat{p}'), \quad (79c)$$

where  $P_L(\cos\theta)$  is the Legendre function for angular momentum  $L$ . After some algebra, we obtain for  $M_2^L$  the expression

$$M_2^t(z, \vec{p}) = \vec{e} \cdot \vec{p} \{ \mathcal{B}_t(z, p) +$$

$$+ 4\pi \sum_{n=s}^t \int_0^{\infty} p'^2 dp' X_{tn}^1(p, p'; z) \tau_n(z - \frac{3p'^2}{4M}) \mathcal{B}_n(z, p') \} \quad (80a)$$

$$\equiv \vec{e} \cdot \vec{p} \mathcal{M}_2^t(z, p) . \quad (80b)$$

The  $\mathcal{B}_s(z, p)$  in Eq.(80) can be obtained in the same manner as  $\mathcal{B}_t(z, p)$  using the projection  $x_2 \bar{n}_1$ ; the result is the same except that  $g_s(k)$  replaces  $g_t(k)$ . The  $X_{tt}^1$  and  $X_{ts}^1$  amplitudes are generated by solving the coupled integral equations

$$X_{nn'}^1(p, p'; z) = Z_{nn'}^1(p, p'; z) + 4\pi \sum_{m=s}^t \int_0^{\infty} p''^2 dp'' Z_{n'm}^1(p', p''; z) \tau_m(z - \frac{3p''^2}{4M}) X_{nm}^1(p, p''; z) , \quad (81)$$

where the driving terms are given by

$$Z_{nn'}^1(p, p'; z) = C_{nn'} \int_{-1}^1 dx \frac{P_1(x) g_n(q^2) g_{n'}(q'^2)}{p^2 + p'^2 + pp'x - Mz} \quad (82)$$

with the coordinate definitions

$$q^2 = \frac{1}{4} p^2 + p'^2 + pp'x , \quad (83a)$$

$$q'^2 = p^2 + \frac{1}{4} p'^2 + pp'x , \quad (83b)$$

$$x = \vec{p} \cdot \vec{p}' / pp' . \quad (83c)$$

Note that we made use of the relation

$$Z_{nn'}^L(p, p'; z) = Z_{n'n}^L(p', p; z) . \quad (84)$$

The spin-isospin coefficient matrix is

$$[C_{nn'}] = \begin{bmatrix} C_{tt} & C_{ts} \\ C_{st} & C_{ss} \end{bmatrix} = \begin{bmatrix} \frac{1}{4} & -\frac{3}{4} \\ -\frac{3}{4} & \frac{1}{4} \end{bmatrix} . \quad (85)$$

Once  $M_2^t(z, \vec{p})$  is obtained, the differential cross section is

constructed in the standard way:

$$d\sigma = 2\pi^2 E_\gamma |\mathcal{M}_2^c (\frac{3p^2}{4M} - \frac{\gamma^2}{M}, p)|^2 \sin^2\theta \rho_f, \quad (86)$$

where  $E_\gamma$  is the photon energy ( $=|\vec{k}|$ ),  $\theta$  is the centre-of-mass angle of the ejected nucleon with respect to the photon direction  $\hat{k}$ , and  $\rho_f$  is the density of final states.

To summarize, we must solve the coupled integral equations given in Eq.(81) for the  $X$  amplitudes. The inhomogeneous terms for these equations are defined by Eq.(82). The resulting  $X_{tt}^1$  and  $X_{ts}^1$  must be combined with the Born amplitudes defined by Eq. (78) and (79a) as indicated in Eqs (80) to obtain  $\mathcal{M}_2^c$  which is required by the cross section expression in Eq.(86).

#### IV. Numerical Methods

How are these equations solved in practice. One method<sup>53</sup> is to solve the coupled integral equations, Eq. (81), for the half-off-shell nucleon-plus-correlated-pair  $X$  amplitudes using standard contour rotation techniques. The variables  $p'$  and  $p''$  are rotated from the real axis into the fourth quadrant:  $p' \rightarrow p' e^{i\phi}$  and  $p'' \rightarrow p'' e^{-i\phi}$ . The rotation angle  $\phi$  is limited by the singularity in the inhomogeneous

term,  $Z_{nn}^1(p, p'; \frac{3p^2}{4M} - \frac{\gamma^2}{M})$ , coming from the energy denominator

$p^2 + p'^2 + pp'x - MZ = 0$ . To avoid this singularity, the rotation angle must be chosen such that

$$\phi < \tan^{-1} \left( \frac{2\gamma}{p} \right). \quad (87)$$

In practice this places a stringent limit on the energy for which contour rotation can be used to solve the separable potential equations.

Having obtained the amplitudes  $X_{tn}^1(p, p' e^{-i\phi}; 3p^2/4M - \gamma^2/M)$ , the amplitude  $M_2^c(3p^2/4M - \gamma^2/M, \vec{p})$  is computed by rotating the  $p'$  integration in the second term on the right-hand-side of Eq. (79a). This is helpful because the bound-state pole  $\omega_{-t}$  is avoided. However, this rotation is possible only if no singularities of  $r_n$  or  $\mathcal{B}_n$  interfere. It is easy to show that this is the case for  $r_n$ : that fact was used in solving Eq. (81). However, the  $\mathcal{B}_n$  are more complicated. Using the fact that the spectator function, i.e. the integral equation generated component of the bound state wave function to be discussed below, can

be fitted very accurately with analytic forms of the type

$$u(p) = (1 + \bar{\alpha}p^2 + \bar{\beta}p^4 + \bar{\gamma}p^6 + \bar{\delta}p^8)^{-1}, \quad (88)$$

one can break  $\mathcal{B}_n$  into a sum of two types of terms: those that require only a single  $k$  integration ( $k = |\vec{k}|$ ) and those that require both a  $k$  integration and an angular integration. Assuming  $p' \rightarrow p'e^{-i\phi}$ , we found that if the  $k$  integration in those terms that do not involve the angular integration are rotated  $45^\circ$  ( $k \rightarrow ke^{-i\pi/4}$ ), then no singularities are encountered. Singularities in the angular-integration terms are avoided by rotating  $k$  the same as  $p'$ , i.e.,  $k \rightarrow ke^{-i\phi}$ . Throughout, it is assumed that for the  $p'$  rotation there is no contribution from the circular arc at infinity. For the integral in Eq. (79a), this can be shown to be true.

The Faddeev amplitude  $\psi_1$  which makes up the S-state component of the wave function has the simple form

$$\psi_1 = N_3 [g_t(k)u_t(p) - g_s(k)u_s(p)] / (k^2 + \frac{3}{4}p^2 + ME_B) \quad (89)$$

where the  $u_n(p)$  are the singlet and triplet spectator functions obtained by means of a homogeneous set of coupled integral equations<sup>59</sup> analogous in form to Eq.(81). These bound-state equations are well known. However, in order to conveniently evaluate  $\hat{V}_p \psi$  as required in the Born terms of Eq.(78), the spectator functions were fitted to the analytic form given in Eq.(88). Barbour and Phillips<sup>48</sup> chose another method for this part of the calculation. Instead of solving for the bound-state wave function using the Hamiltonian that generated the continuum wave function, they assumed a form like that generated by S-wave separable interactions, set the binding energy to the experimental value, and used the rms radius to fix the remaining parameter defining the spectator function. Such a phenomenological approach overemphasizes the asymptotic region. When combined with the E1 operator, this leads to a significant overestimate of the cross section near the peak. We shall return to this point in the next section.

## V. Sample Numerical Results

The most important feature of the two-body photodisintegration cross section is the enhancement in the peak region of the full calculation over the plane wave Born approximation (PWBA), as shown in the  $90^\circ$  differential cross sections in Fig.24. The peak cross section for the full calculation is 40-50% larger. This type of effect was first reported in Ref. 48. However, the fascinating reason for this

enhancement was not clear until the publication of Ref. 53. There it was shown that the on-shell distorted wave Born approximation result (DWBA) was actually smaller than the PWBA. On-shell neutron-deuteron final-state rescattering reduces the cross section  $\sim 10\%$ , not increases it. Furthermore, retaining the off-shell rescattering in the triplet neutron-deuteron amplitude does not account for the large enhancement. The enhancement in the full amplitude comes from the off-shell scattering in the singlet correlated-pair-plus-nucleon intermediate state that leads to an on-shell neutron-plus-deuteron final state.

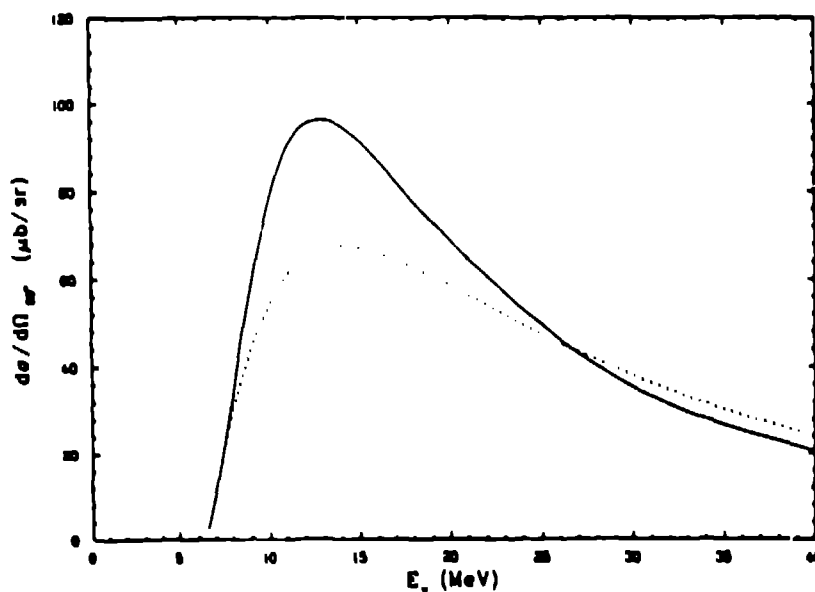


Fig. 24. Comparison of the  ${}^3\text{H}(\gamma, d)n$   $90^\circ$  differential cross section calculated with the complete solution of the separable potential equation (solid curve) with the plane wave Born approximation for the same model.

That is, the enhancement comes from an  $N+d^*$  rescattering which takes the  $d^*$  to a physical  $d$ . The two-body breakup channel is absorbing strength from the three-body breakup channel. This is possible only in a formalism that properly includes three-body unitarity. The two-body and  $T=1/2$  three-body breakup channels are not independent. Their intimate connection cannot be ignored. Exact equation approaches were needed to understand the physics.

Data for the  ${}^3\text{H}(\gamma, n)d$  reaction total cross section are shown Fig.25. In the electric dipole approximation, the total cross section is  $8\pi/3$  times the  $90^\circ$  differential cross section. Thus the model calculations are qualitatively correct, which is all one can hope for in the simple model we have constructed. The comparison of the model with the data is better seen in a study of  ${}^3\text{He}(\gamma, p)d$  shown in

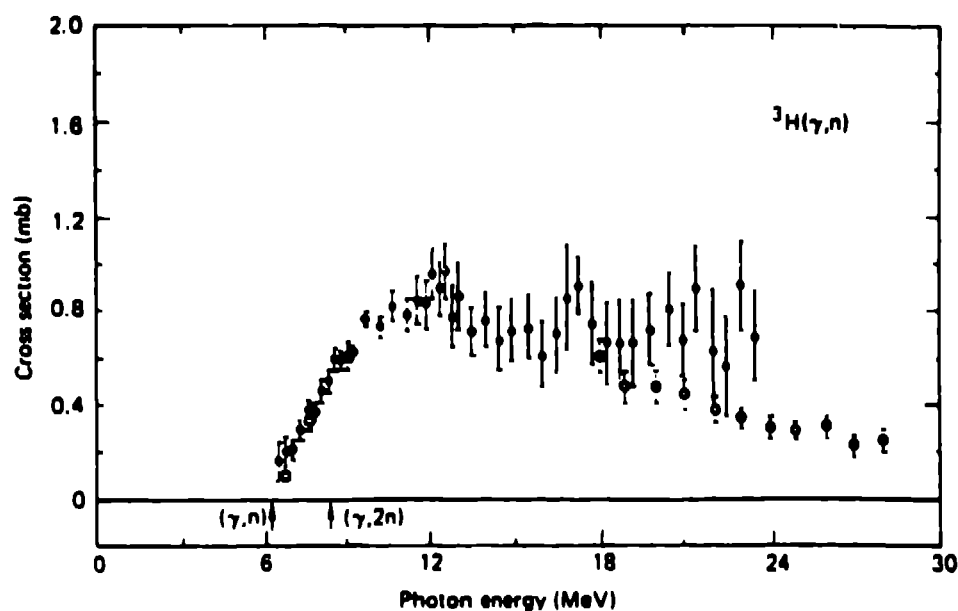


Fig. 25. The total cross section for the  ${}^3\text{H}(\gamma,n)d$  reaction as reported in Ref. 60.

Fig. 26. Here the solid curve gives quite a reasonable representation of the data. The dashed curve is a calculation performed within the context of this model but using the Ref. 48 prescription for constructing a phenomenological ground-state wave function. Recall that the correct analytic form was used; the binding energy was

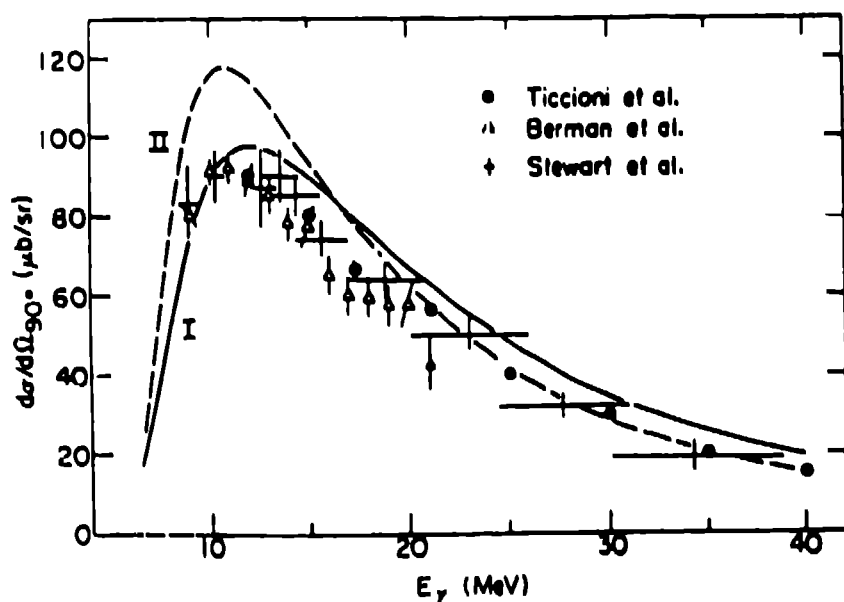


Fig. 26. Comparison of selected  ${}^3\text{He}(\gamma,d)p$   $90^\circ$  differential cross section data (Ref. 61) with the calculations of Ref. 53 (solid curve) and Ref. 48.

determining the spectator function was fitted to the rms radius. On the basis of such a curve, Barbour and Phillips concluded that the photodisintegration data were incompatible with the rms radius of  $^3\text{He}$ . A better conclusion from Fig.26 is that one should use ground-state and continuum wave functions generated by the same Hamiltonian. Approximations in physics can be tricky and are often difficult to justify a priori.

In summary, we have examined a very simple model calculation of the two-body photodisintegration of  $^3\text{H}$  but one which encompasses much of the important physics. We have seen how to produce a calculation from an abstract theory. Finally, we have examined the solution to part of what was once a real puzzle in photonuclear physics:<sup>47,50</sup> Why was the two-body cross section so large (compared to the three-body cross section)?

### Acknowledgements

The work of the author is performed under the auspices of the U.S. Department of Energy. The author would like to thank his collaborators, J.L. Friar, G.L. Payne, and D. R. Lehman, for their assistance in compiling these lectures. Finally, the author wishes to thank the School of Physics at Melbourne University for its hospitality during the preparation of the manuscript and in particular Mrs. E. Smart for her technical assistance in that task.

### Appendix A. Jacobi Coordinates

The centre-of-mass Jacobi coordinates in configuration space are defined by

$$\hat{x}_1 = \hat{r}_j - \hat{r}_k \quad (\text{A1a})$$

and

$$\hat{y}_1 = \frac{1}{2} (\hat{r}_j + \hat{r}_k) - \hat{r}_l \quad (\text{A1b})$$

The  $r_l$  are the coordinates of nucleon  $l$ , and the subscripts are to be taken cyclically. We will choose the pair  $(x_1, y_1)$  shown in Fig.A1 to be the coordinates  $(x, y)$  with which we define our wave functions and amplitudes. The other two pairs can then be expressed in terms of  $\hat{x}$  and  $\hat{y}$  by the relations

$$\hat{x}_2 = \frac{1}{2} \hat{x} + \hat{y} \quad (\text{A2a})$$

## Appendix B. Spin-Isospin Formalism

The doublet spin states for three nucleons have the form

$$x_1 = |1, \frac{1}{2}, \frac{1}{2}\rangle \quad (B1a)$$

$$= \frac{1}{\sqrt{6}} [ (++) + (+-) - 2 (-++) ] \quad (B1b)$$

$$x_2 = |1, 0, \frac{1}{2}\rangle \quad (B1c)$$

$$= \frac{1}{\sqrt{2}} [ (++) - (+-) ] \quad (B1d)$$

Here a + (or -) means that the nucleon corresponding to that position has spin up (or down). Similarly, the isospin functions  $n_1$  and  $n_2$  can be defined to have the forms in Eqs.(B1) where a + (or -) means that the nucleon is a proton (or neutron); such functions describe  $^3\text{He}$  and  $^3\text{H}$  functions are obtained by interchanging + and - in the  $n$ 's.

The spin-isospin basis states are linear combinations of these  $x$ 's and  $n$ 's. The combinations which we require are

$$\phi_a = \frac{1}{\sqrt{2}} (x_1 n_2 - x_2 n_1) \quad (B2a)$$

$$\phi_1 = \frac{1}{\sqrt{2}} (x_2 n_2 - x_1 n_1) \quad (B2b)$$

$$\phi_2 = \frac{1}{\sqrt{2}} (x_2 n_1 + x_1 n_2) \quad (B2c)$$

The function  $\phi_a$  is fully antisymmetric under the interchange of any two nucleons, while  $\phi_1$  and  $\phi_2$  have the same mixed symmetry properties as do the  $x$ 's and  $n$ 's.

The Pauli principle requires that the overall wave function be fully antisymmetric in the interchange of all coordinates of any pair of nucleons. The function  $\phi_a u$  satisfies this requirement, where  $u$  is spatially symmetric. This is the  $^2S_{1/2}$  component of  $\psi$ , which is denoted by  $S$ . Combinations of  $\phi_1$  and  $\phi_2$  with spatial functions of mixed symmetry that describe the trinucleons must also possess the  $\phi_a$  antisymmetry property. There is one:  $\phi_1 v_2 - \phi_2 v_1$ . This is the  $^2S_{1/2}$  state of mixed symmetry which is denoted by  $S'$ . The full wave function is then of the form

$$\psi = \phi_a u + (\phi_1 v_2 - \phi_2 v_1) \quad (B3)$$

Over 10 years ago pion-exchange current contributions to the charge density operator were calculated and then later applied in the case of  $^3\text{He}$ . (See Ref.33.) Effects were found which were of the right sign and of sufficient magnitude to resolve the disagreement between theory and experiment concerning the size and shape of the charge form factor. Friar,<sup>13</sup> however, showed about the same time that these corrections to the charge density operator (1) are relativistic corrections [i.e.,  $(v/c)^2$  compared to 1], (2) contain important momentum-dependent terms which have never been included in  $^3\text{He}$  calculations, (3) are model dependent, reflecting the physical difference between pseudoscalar and pseudovector couplings of pions and nucleons,<sup>39</sup> and (4) are ambiguous, reflecting a unitary ambiguity which arises in different methods of calculating these operators.

The fact that these isoscalar exchange currents are of relativistic origin means that one must do a relativistic calculation (including refitting the nucleon-nucleon interactions to the two-body data) to include them in a meaningful wave. The pseudoscalar versus pseudovector coupling model dependence is unavoidable. The unitary ambiguity is vexing because it would vanish if the wave functions calculated with a given potential were used with a commensurate form of the charge operator - such matrix elements could be free of any ambiguity. But realistic potentials to date have the wrong form to correspond to any of the allowed unitary representations of the charge density operator.

Exchange currents of the isovector ilk are not relativistic corrections compared to the nuclear current,  $\vec{p}/M$ . They contribute in a non-negligible manner to the magnetic density form factors of the trinucleons. Friar has discussed these in great detail.<sup>13</sup> See also the exchange current references in the magnetic moment investigation of Ref.40.

1. N.F. Mott, Proc. Roy. Soc. (London) A124 (1929) 426; A135 (1932) 429.
2. M.E. Rose, Phys. Rev. 73 (1949) 279.
3. R. Hofstadter, Rev. Mod. Phys. 28 (1956) 214; Ann. Rev. Nucl. Sci. 7 (1957) 231.
4. R.A. Malfliet and J.A. Tjon, Nucl. Phys. A127 (1969) 161.
5. J.L. Friar, B.F. Gibson, and G.L. Payne, Z. Phys. A301 (1981) 309.
6. D.R. Yennie, D.G. Ravenhall, and R.N. Wilson, Phys. Rev. 95 (1954) 500.

7. J.L. Friar, B.F. Gibson, and G.L. Payne, Phys. Rev. C22 (1980) 284.
8. J.L. Friar, B.F. Gibson, and G.L. Payne, Z. Phys. A312 (1983) 169.
9. J.D. Bjorken and S.D. Drell, Relativistic Quantum Mechanics, (McGraw-Hill, New York, 1964) ch.7.
10. G. Hoehler et al., Nucl. Phys. B114 (1976) 505.
11. L.I. Schiff, Phys. Rev. 92 (1953) 988.
12. L.I. Schiff, Phys. Rev. 133 (1964) B802.
13. J.L. Friar, Ann. Phys. (N.Y.) 104 (1977) 380; Phys. Lett. 59B (1975) 145; in New Vistas in Electronuclear Physics (Plenum, New York, 1986).
14. B.F. Gibson, Proceedings of the International Conference on Photonuclear Reactions and Applications, ed. by B.L. Berman (Lawrence Livermore Laboratory, CONF-730301, 1973) p 373.
15. J.A. Tjon, B.F. Gibson, and J.S. O'Connell, Phys. Rev. Lett. 25 (1970) 540.
16. J. Martino, Proceedings of the International Symposium on the Three-Body Force in the Three-Body System, ed. by B.L. Berman and B.F. Gibson, in Lecture Notes in Physics (Springer-Verlag, Heidelberg, 1986) Vol.260.
17. J.L. Friar, B.F. Gibson, C.R. Chen, and G.L. Payne, Phys. Lett. 161B (1985) 241.
18. C.R. Chen, G.L. Payne, J.L. Friar, and B.F. Gibson, Phys. Rev. C 31 (1985) 2266.
19. C.R. Chen, G.L. Payne, J.L. Friar, and B.F. Gibson, Phys. Rev. C 33 (1986) 1740.
20. J.L. Friar, B.F. Gibson, G.L. Payne, and C.R. Chen, Phys. Rev. C 34 (1986).
21. F.-P. Juster et al., Phys. Rev. Lett. 55 (1985) 2261; S. Platchkov and B. Frois, private communication.
22. R.V. Reid, Ann. Phys. (N.Y.) 50 (1968) 411; B.D. Day, Phys. Rev. C 24 (1981) 1203, provides the higher partial waves.
23. R.B. Wiringa, R.A. Smith, and T.L. Ainsworth, Phys. Rev. C 29 (1984) 1207.
24. R. de Tourreil and D.W.L. Sprung, Nucl. Phys. A201 (1973) 193.
25. R. de Tourreil, B. Rouben, and D.W.L. Sprung, Nucl. Phys. A242 (1975) 445.
26. S.A. Coon, M.D. Scadron, P.C. McNamee, B.R. Barrett, D.W.E. Blatt, and B.H.J. McKellar, Nucl. Phys. A317 (1979) 242.
27. H.T. Coelho, T.K. Das, and M.R. Robilotta, Phys. Rev. C 28 (1983) 1812.
28. J. Carlson, V.R. Pandharipande, and R.B. Wiringa, Nucl. Phys. A401 (1983) 59; R.B. Wiringa, ibid A401 (1983) 86.
29. H. Collard et al., Phys. Rev. 138 (1965) B57.
30. J.S. McCarthy, I. Sick, R.R. Whitney, and M.R. Yearian, Phys. Rev. Lett. 25 (1970) 884; J.S. McCarthy, I. Sick, and R.R. Whitney, Phys. Rev. C 15 (1977) 1396; R.G. Arnold et al., Phys. Rev. Lett. 40 (1978) 1429.
31. D.H. Heck, J. Asai, and D.M. Skopik, Phys. Rev. C 25 (1982) 1152; D.H. Beck, et al., ibid 30 (1984) 1403; D.H. Beck, private communication.
32. J.M. Cavedon et al., Phys. Rev. Lett. 49 (1982) 986; P.C. Dunn et al., Phys. Rev. C 27 (1983) 71; G.A. Retzlaff and D.M. Skopik, ibid 29 (1984) T194; C.R. Otterman et al., Nucl. Phys. A436 (1985) 688.
33. W.M. Kloet and J.A. Tjon, Phys. Lett. 49B (1974) 419; E. Hadjimichael, R. Bornais, and R. Goulard, Phys. Rev. Lett. 48 (1982) 583; Phys. Rev. C 27 (1983) 831; T. Sasaki, A. Fukunaga, and S. Ishikawa, Czechoslovak Journal of Physics B36 (1986) 312.
34. I. Sick, in Lecture Notes in Physics (Springer-Verlag, Berlin, 1978) Vol. 87, p236.

35. J.L. Friar, Nucl. Phys. A150 (1970) 45.
36. M. Fabre de la Ripelle, Fizika 4 (1972) 1.
37. M. Fabre de la Ripelle, Prog. Theor. Phys. 40 (1968) 1454; Rev. Bras. Fis. (Suppl.) (1980) 219.
38. J.L. Friar and B.F. Gibson, Phys. Rev. C 15 (1977) 1779.
40. E.L. Tomusiak, M. Kimura, J.L. Friar, B.F. Gibson, G.L. Payne, and J. Dubach, Phys. Rev. C 32 (1985) 2075.
41. C. Chadwick and M. Goldhaber, Nature 134 (1935) 237.
42. G.E. Brown and D.O. Riska, Phys. Lett. 38B (1972) 193; M. Garl and A.H. Hoffman, Phys. Rev. C 1 (1973) 994.
43. J.S. Merritt, J.G.V. Taylor, and A.W. Boyd, Nucl. Sci. Eng. 34 (1968) 195; E.T. Jurney et al., Phys. Rev. C 25 (1982) 2810.
44. L.I. Schiff, Phys. Rev. 52 (1937) 149; A.C. Phillips, Phys. Rev. 170 (1968) 952; Nucl. Phys. A184 (1972) 337.
45. R.J. Hughes et al., Nucl. Phys. A267 (1976) 329; J.F. Gilot et al., Phys. Lett. 47 (1981) 304; H.O. Meyer et al., Phys. Rev. Lett. 52 (1984) 1759.
46. A. Cambi, B. Mosconi, and P. Ricci, Phys. Rev. Lett. 48 (1982) 462; J. Phys. G10 (1984) L11; J.L. Friar, B.F. Gibson, and G.L. Payne, Phys. Rev. C 30 (1984) 441.
47. G. Barton, Nucl. Phys. A104 (1967) 189.
48. I.M. Barbour and A.C. Phillips, Phys. Rev. C 1 (1970) 165.
49. B.F. Gibson and D.R. Lehman, Phys. Rev. C 13 (1976) 477.
50. B.F. Gibson, Nucl. Phys. A353 (1981) 85c.
51. J.R. Calarco et al., Phys. Rev. C 27 (1983) 1866; B.L. Berman et al., Phys. Rev. C 22 (1980) 2273; L. Ward et al., Phys. Rev. C 24 (1981) 317.
52. B.F. Gibson, Nucl. Phys. A195 (1972) 449.
53. B.F. Gibson and D.R. Lehman, Phys. Rev. C 11 (1975) 29.
54. E.O. Alt, P. Grassberger, and W. Sandhas, Nucl. Phys. B2 (1967) 167.
55. I.M. Barbour and J.A. Hendry, Phys. Lett. 38B (1972) 151.
56. A.J.F. Siegert, Phys. Rev. 52 (1937) 787.
57. Y. Yamaguchi, Phys. Rev. 95 (1955) 1628.
58. J.H. Herberington and L.M. Schick, Phys. Rev. 137 (1965) B935; 156 (1967) 1647.
59. B.F. Gibson and G.J. Stephenson, Jr., Phys. Rev. C 8 (1973) 1222; A.G. Sitenko and V.F. Kharchenko, Nucl. Phys. 49 (1963) 15.
60. D.D. Faul et al., Phys. Rev. Lett. 44 (1980) 129; Phys. Rev. C 24 (1981) 849.
61. J.R. Stewart, R.C. Morrison, and J.S. O'Connell, Phys. Rev. 138 (1965) B372; B.L. Berman, L.J. Keoster, and J.H. Smith, Phys. Rev. 133 (1964) B117; G. Ticcioni et al., Phys. Lett. 46B (1973) 369.